JAERI - M
90-072

REPORT OF THE SEMINAR ON NUCLEAR PHYSICS AND ATOMIC PHYSICS AT THE JAERI TANDEM-BOOSTER ACCELERATOR

April 1990

(Eds.) Hiroshi IKEZOE, Yuichiro NAGAME and Masao SATAKA

日 本 原 子 力 研 究 所
Japan Atomic Energy Research Institute

JAERI-Mレポートは，日本原子力研究所が不定期に公刊している研究報告書です。
入手の問合わせは，日本原子力研究所技術情報部情報資料課（〒319-11茨城県那珂郡東海村）あて，お申しこしください。なお，このほかに財団法人原子力弘済会資料センター（〒319-11 茨城県那珂郡東海村日本原子力研究所内）で複写による実費頒布をおこなっております。

JAERI-M reports are issued irregularly.
Inquiries about availability of the reports should be addressed to Information Division, Department of Technical Information, Japan Atomic Energy Research Institute, Tokai-mura, Naka-gun, Ibaraki-ken 319-11, Japan.

編集兼発行　日本原子力研究所
印　　刷　㈱原子力資料サービス

JAERI-M 90-072

Report of the Seminar on Nuclear Physics and Atomic Physics at the JAERI Tandem-Booster Accelerator

(Eds.) Hiroshi IKEZOE, Yuichiro NAGAME[+] and Masao SATAKA

Department of Physics
Tokai Research Establishment
Japan Atomic Energy Research Institute
Tokai-mura, Naka-gun, Ibaraki-ken

(Received March 16, 1990)

A meeting on new experimental apparatus which are suitable for Nuclear Physics and Atomic Physics at the JAERI tandem-booster accelerator beeing under construction was held at Tokai Research Establishment of JAERI in the period from 6 to 7 November, 1989. More than 80 participants from universities and JAERI attended to discuss the following themes:

1. Atomic and Molecular Physics in the energy region of tandem-booster accelerator.
2. Experimental methods and apparatus for nucler structure study.
3. Experimental methods and apparatus for nuclear reaction study.

Keywords: Heavy-Ion, Tandem-Booster Accelerator, High Spin, Crystal Ball, Nuclear Structure, Recoil Mass Separator, One-Line Mass

---

Members of Organizing Committee: H. Ikezoe, Y. Nagame and M. Sataka.
+ Department of Radioisotopes

JAERI－M 90－072

原研タンデム・ブースター加速器での核物理・原子分子物理研究会
報　　告　　集

日本原子力研究所東海研究所物理部
（編）池添　博・永目諭一郎・左高　正雄

（1990年3月16日受理）

現在建設中のタンデム・ブースター加速器を使った核物理・原子分子物理の実験装置としてどの様なものが可能であり，建設すべきであるかを検討するため，「原研タンデム・ブースター加速器での核物理・原子分子物理研究会」が1989年11月6日及び7日に日本原子力研究所東海研究所に於て開催された。所内及び所外の各大学から84人の研究者が参加して討論がおこなわれた。この報告集は，研究会で発表された研究報告をまとめたものである。

本研究会の世話人は，池添　博，永目諭一郎，左高　正雄が担当した。

東海研麻所：〒319－11 茨城県那珂郡東海村白方字白根2－4
＋アイソトープ部

Contents

目　　次

1. Project of the JAERI Tandem Booster and Its Status

S. Takeuchi
Department of Physics, Japan Atomic Energy Research Institute,
Tokai Establishment

The project of developing a superconducting booster for the JAERI tandem accelerator was proposed and initiated by N. Shikazono in 1982 in order to increase the useful region of heavy ions for nuclear reactions, which has been limited below about 70 a.m.u., toward the region up to uranium.

The development work has been proceeding successfully. A prototype quarter wave coaxial line resonator(QWR) made of niobium and copper was developed. It showed so good performance that niobium QWRs will be a very promising accelerating structure for heavy ions. Two units, each of which is composed of two QWRs, have been built for a buncher and a de-buncher of the booster. The technology of the superconducting QWRs has been established in these works. The booster linac will be composed of forty QWRs. The QWR's optimum beam velocity is 0.1c and the threshold velocity is 0.045c. As a result of tests with the resonators already built, the available acceleration voltage has been found to be 0.75 MV or more for the optimum beam velocity. That is, we can expect an accleration voltage of about 30 MV from the booster linac. The fabrication of the linac is proceeding in a factory of Mitsubishi Electric Co.

The layout plan of the booster is shown in Fig.1. The buncher, the linac, the de-buncher and the analyzing magnet will be lined up on the straight line from the tandem analayzing magnet. The buncher will be composed of 130 MHz QWRs and 260 QWRs. It will be able to bunch about 60 % of the dc beams from the tandem. The 130 MHz beam bunches will be accelerated in ten linac units, each of which houses four 130MHz QWRs and is accompanied with a normal conducting magnetic quadrupole doublet lens. The accelerated beam bunches will be elongated in time by a drift of 10 m and crushed in energy by the de-buncher. Unbunched and out-of-phase beams will be swept away by the analyzing magnet. High quality cw beams of about 1 ns in length and 7.7 ns in period will be delivered to the new target area. A re-buncher may be necessary for experiments which need sharp timing. A low frquency buncher or sweeper

may be also necessary. Such units are not involved in the present project, unfortunately.

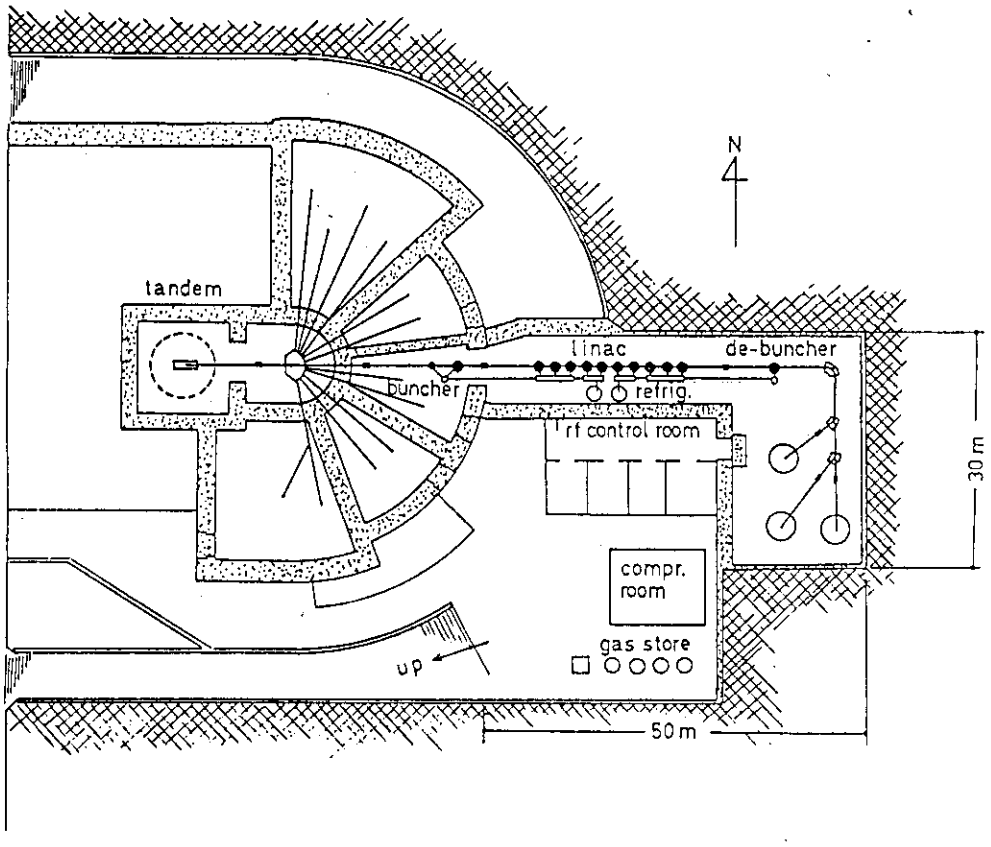

Fig. 1 Layout plan of the JAERI tandem booster.

The energy performance expected for the booster is shown in Fig.2. Very heavy ions such as gold or bismuth ions, will be useful for nuclear experiments. In case of using gas stripper at the tandem terminal for very heavy ions, the second foil stripper which is located 2/3 of the column of the tandem(F2) will be used instead of the post tandem foil stripper(F3), although it results in lower energy output. The beam current reduces by a factor of ten compared to the present level, due to a use of additional stripper(F2 or F3) and the bunching efficiency of about 60 %. The beam current from the booster is expected to be an order of 1 or 10 pnA for most heavy ions.

To complete the present project, it will take about 3 more years. The booster building will be built in 1991. Majour components of the booster will be installed in 1992. We will hopefully try the first beam acceleration in the beginning of 1993.

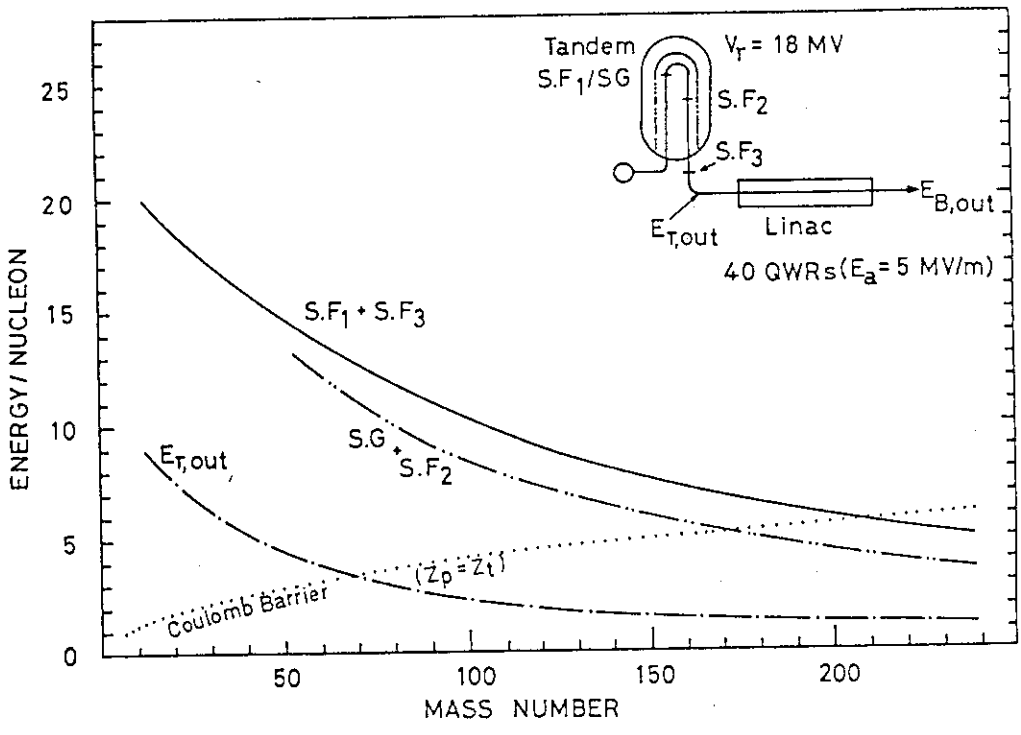

Fig. 2 Energy performance of the JAERI tandem booster.

2. Calculation of One-dimensional Stopping Power due to the Dielectric Response Method

Mitsuo Kitagawa

Department of Electronics, North Shore College

Atsugi 243, Japan

1. Dielectric function in inhomogeneous many-electron systems

The first order of analytical formula for the dielectric function ε in $\vec{r}$-ω space, which is proportional to $1/\omega^2$, was represented as follows[1)]

$$\begin{aligned}\varepsilon(\vec{r}_1,\vec{r}_2,\omega) &= \delta(\vec{r}_1-\vec{r}_2) + \frac{1}{m\omega^2}\,\mathrm{div}_{\vec{r}_1}\left[\left(\mathrm{grad}_{\vec{r}_1}\frac{e^2}{|\vec{r}_1-\vec{r}_2|}\right)n(\vec{r}_1)\right] \\ &= \delta(\vec{r}_1-\vec{r}_2)\left(1-\frac{4\pi e^2 n(\vec{r}_1)}{m\omega^2}\right) - \frac{e^2(\vec{r}_1-\vec{r}_2)}{m\omega^2|\vec{r}_1-\vec{r}_2|^3}\,\mathrm{grad}_{\vec{r}_1}n(\vec{r}_1).\end{aligned} \tag{1}$$

In the above, $\vec{r}_1$ and $\vec{r}_2$ refer to the position vectors, and $n(\vec{r}_1)$ indicates the electron density at $\vec{r}_1$. $\omega_p(\vec{r}_1)(=[4\pi e^2 n(\vec{r}_1)/m]^{1/2})$ is the plasmon type localized mode. Also we obtain the inverse dielectric function ε^{-1} through the integral equation derived from the orthogonality ε and ε^{-1}. Applying an iteration to the above integral equation, we obtain the first order of analytical formula for ε^{-1} as follows[1)]

$$\begin{aligned}\varepsilon^{-1}(\vec{r}_1,\vec{r}_2,\omega) \fallingdotseq \frac{\omega^2}{\omega^2-\omega_p^2(\vec{r}_1)}\Bigg[\delta(\vec{r}_1-\vec{r}_2) \\ - \frac{e^2}{m}\,\frac{1}{\omega^2-\omega_p^2(\vec{r}_1)}\,\frac{(\vec{r}_1-\vec{r}_2)}{|\vec{r}_1-\vec{r}_2|^3}\,\mathrm{grad}_{\vec{r}_1}n(\vec{r}_1)\Bigg].\end{aligned} \tag{2}$$

2. Stopping power for one dimensional case

By use of the electro-magnetic theory, the stopping power S is given as follows

$$S = -Z_1 e \, \mathrm{grad}_{\vec{r}_1} \phi(1)|_{\vec{r}_1=\vec{r}_b} \cdot \frac{\vec{V}}{V} \quad , \tag{3}$$

$$\phi(1) = \int v(13)[\varepsilon^{-1}(32) - \delta(32)]\rho^{ext}(2)d(23) \quad , \tag{4}$$

$$\rho^{ext}(2) = \delta(\vec{r}_2 - \vec{r}_b) \quad [\vec{r}_b = (\vec{b}, Vt_2)] \quad . \tag{5}$$

In eqs.(3)-(5), $\phi(1)$ indicates the potential from the polarization cloud, in which the second term denotes the subtraction of the pure Coulomb part because such a part doesn't contribute to the energy loss process. $\rho^{ext}(2)$ indicates the number density of external charge if we consider a classically straight trajectory of the projectile. $\vec{V}$ and $\vec{b}$ denote the velocity and the impact parameter of the projectile.

We consider the system, in which the electron density is treated to change one-dimensionally in order to derive the stopping power formula for the cases of the surface and planar channeling. We take the electron density n in inhomogeneous system as a function of x, and $\vec{r}_b$ in eq.(5) as $(b,0,Vt_2)$. After several kinds of calculations, we have the integral formula of stopping power for the case of the one-dimensional problem[2]

$$S = \frac{(Z_1 e)^2}{V^2}\{\omega_p^2(b)\log\left(\frac{q_{max}V}{\omega_p(b)} + \sqrt{\frac{q_{max}^2V^2}{\omega_p^2(b)} + 1}\right) - \frac{1}{2}\int dx \, \frac{\partial \omega_p^2(b)}{\partial x} \, \frac{b-x}{|b-x|}$$

$$\times P\left(\frac{1}{\omega_p^2(b) - \omega_p^2(x)}\right)\left[\omega_p^2(b)\int_0^{q_{max}} \frac{dq}{\sqrt{q^2 + (\omega_p(b)/V)^2}} \, e^{-2|x-b|\sqrt{q^2+(\omega_p(b)/V)^2}}\right.$$

$$\left. - \omega_p^2(x)\int_0^{q_{max}} \frac{dq}{\sqrt{q^2 + (\omega_p(x)/V)^2}} \, e^{-2|x-b|\sqrt{q^2+(\omega_p(x)/V)^2}}\right]\} \quad . \tag{6}$$

Here q_{max} corresponds to the maximum momentum transfer for the process discussed here. If we take $\hbar q_{max} = mV$ and consider the case of $q_{max}V/\omega_p(b) \gg 1$, the first term in eq.(6) is reduced to the usual Bethe formula. We note that eq.(21) includes the arbitrary function of the electron density. Therefore, it is possible to apply the above formula to a one-dimensionally

inhomogeneous system, for example, the surface and planar channeling problems.

Now, we consider the planar uniform-background model for the surface, in which we take the electron density $n(x)=n_0\theta(-x)$, where θ is the Heaviside step function. In this case, we can easily perform the integration over x in eq.(6) and get the result as follows

$$S = \frac{(Z_1 e)^2}{V^2}\{\omega_p^2\theta(-b)\log\left(\frac{q_{max}V}{\omega_p} + \sqrt{\frac{q_{max}^2V^2}{\omega_p^2}+1}\right) + \omega_s^2\int_0^{q_{max}}\frac{dq}{\sqrt{q^2+(\omega_s/V)^2}}\,e^{-2|b|\sqrt{q^2+(\omega_s/V)^2}} - \omega_p^2\theta(-b)\int_0^{q_{max}}\frac{dq}{\sqrt{q^2+(\omega_p/V)^2}}\,e^{-2|b|\sqrt{q^2+(\omega_p/V)^2}}]\} \quad . \tag{7}$$

In eq.(7), ω_s and ω_p denote the well-known frequency of surface and bulk plasmons. Eq.(7) is in agreement with the expression by Kawai et al.[3], if we define $q_{max}=[q_c^2-(\omega_{p(s)}/V)^2]^{1/2}$, where q_c is the cutoff wave number of plasmons. If we make the approximation of $q_{max}\rightarrow\infty$ in the above integrals, we also get the same expression by Núñez et al.[4].

From the above results, we confirm the usefulness of eq.(6) in solving the one-dimensional problem for the inhomogeneous many-electron system, for example, the energy loss in cases of surface and planar channeling.

References

(1) M. Kitagawa, Nucl. Instr. and Meth. B13 (1986) 133.

(2) M. Kitagawa, Nucl. Instr. and Meth. B33 (1988) 409.

(3) R. Kawai, N. Itoh and Y.H. Ohtsuki, Surf. Sci. 114 (1982) 137.

(4) R. Núñez, P.M. Echenique and R.H. Ritchie, J. Phys. C13 (1980) 4229.

3. ON THE OKOROKOV EFFECT

Hideo Nitta

Department of Physics, Tokyo Gakugei University

1. Introduction

When energetic ions enter a crystal pararel to a major axis, the ions feel periodic field with a period $T_r = d/v$, where d is the interatomic distance of the atomic string, and v is the speed of the incident ion. The origin of the periodic field is the atomic potential periodically located on the string. If an excitation energy of the ion $E_2 - E_1$ coincides with the frequency of the periodic field $\omega_r = 2\pi/T_r$, the ion may be excited in a resonant manner. This special effect under channeling condition is called the "coherent resonant excitation" or the "Okorokov effect".

The Okorokov effect was predicted by Okorokov in 1965[1] and confirmed experimentally by Datz et al.[2] and Iwata et al.[3]. In this report we will give an outline of the theory of the Okorokov effect.

2. Okorokov Condition

Because of the periodic structure of the atomic string, the static potential for channeled particles can be expanded in a Fourier series over reciprocal lattice vectors g,

$$V(\boldsymbol{r}) = V_0(\boldsymbol{b}) + \sum_g V_g(\boldsymbol{b})\, e^{igz} \qquad (1)$$

where z is the direction parallel to the atomic string, b is the impact parameter, and $g = 2\pi m/d$ $(m = \pm 1, \pm 2, \cdots)$. The Oth Fourier component $V_0(b)$ is nothing but the Lindhard's continuum potential[4]:

$$V_0(\boldsymbol{b}) = \frac{1}{L}\int V(\boldsymbol{r})\, dz$$

where L is the crystal thickness. As shown by Lindhard[4], channeling motion is well described by the continuum potential or the first term on

the r.h.s. of eq.(1). Usually, the second term of eq.(2) can be neglected. However, when the channeled particle has some internal degree of freedom, the Okorokov effect may occur due to the existence of the second term of eq.(1). Considering a well channeled particle and neglecting its energy loss, we have $z = v\ t$ and get a time-dependent perturbation potential from the second term of eq.(1):

$$H'\ (\boldsymbol{b},\ t)\ = \sum_{m} V_m\ (\boldsymbol{b})\ exp\ (i m \omega_r\ t) \qquad (2)$$

Therefore, if the channeled particle has an internal degree of freedom for which excitation energy $E_2 - E_1$ is equal to $m\hbar\omega_r$, it will be resonantly excited due to the periodic force caused by the mth Fourier component in eq.(2). From other point of view, the Okorokov effect appears when the channeled particle has velocity $v = v_r$;

$$v_r = \left(\frac{d}{2\pi}\right)\frac{(E_2 - E_1)}{m} \qquad (m = 1, 2, \cdots) \qquad (3)$$

Eq.(3) is called the Okorokov condition.

For a hydrogenic ion in vacuum, the energy levels are given by

$$E_n = -\frac{Z_1\ e^2}{2\ a_B\ n^2} \qquad (4)$$

where Z_1 is the atomic number of the ion and a_B is the Bohr radius. Using eqs.(3) and (4), we can calculate Okorokov conditions.

Experiments have confirmed that channeled ions are strongly excited near the Okorokov conditions. However, it was observed that the Okorokov peak profiles have structures and widths[2] which are ascribed to interactions between channeled ions and the crystal. We will briefly discuss them in the next section.

3. *Energy Level of Channeled Ions*

3.1 Level shift

When the ion enters the crystal, because of the presence of the potentials inside the crystal, the ion states are modified just like the Stark effect[5]. The continuum potential $V_0(b)$ and the dynamical potential V_d produced by electron wake give the dominant contributions.

These potentials remove the degeneracy of the excited states. Neskovic[6] showed that the hydrogenic $n=2$ states are split into four nondegenerate states. The order of magnitude of the energy shifts ΔE_2 is $\Delta E_2/E_2 \sim 1\%$. By Monte-Carlo simulations, Neskovic got a good agreement of the Okorokov peak positions with experimental results[6]. However, the line widths of the Okorokov peaks have not been explained.

3.2 Level broadening

There are some possible origins of the level broadening of the Okorokov peaks. The finite thickness of the crystal limits the coherence of the Okorokov effects and results broadening. Shindo and Ohtsuki[7] pointed out that the dynamical effect like as electron diffraction may cause width of the Okorokov peaks. However, these contributions have turned out to be the order of magnitude smaller than the experimental values. Thus, we have to consider another mechanism which gives the major contributions to the line width of the Okorokov effect.

Channeled ions collide with the various degrees of freedom in the crystal. As a result, the energy levels of the channeled ions E_n have finite lifetimes τ_n. Thus, due to the uncertainty principle, the energy levels have widths determined by $\delta E_n = \hbar/\tau_n$.

τ_n^{-1} represents the inelastic scattering probability of nth state per unit time and we can calculate it by means of first order perturbation. However, under channeling conditions, the impact parameter dependence is generally very important and we should calculate a position-dependent inelastic scattering probability $w_n(b)$. The significant contributions to τ_n^{-1} is the scattering by thermally displaced target nuclei (phonon scattering) and the scattering by target electrons. In an amorphous target, scattering probability by nuclei $w_{am}^{(n)}$ is much larger than that by electrons $w_{am}^{(e)}$: $w_{am}^{(n)} \sim Z_2 w_{am}^{(e)}$. However, since $w^{(n)}(b)$ is strongly localized to the atomic string, its contribution to the inelastic scattering probability for well channeled ions will become much smaller.

A Theory of the level broadening by using an impact parameter method has been developed by the present author and Shindo[8].

4. *Concluding Remarks*

The Okorokov effect is not only possible for excitations of atomic states but also for any of internal degrees of freedom in channeled particles. Actually, nuclear Okorokov effects have been proposed[1)9)]. In this case, the velocity of channeled particle becomes relativistic and we should substitute d in the Okorokov conditions eq.(3) by d/γ where γ is the Lorentz factor. Recently, Okorokov discussed the possibility of the excitations of hadrons of which the Okorokov conditions require the energy of channeled hadrons of the order of 1~10TeV[10)]!

Finally, it is worthwhile to point out that the Okorokov effect is not only interesting in terms of investigating various kind of beam-solid interactions but also as a possible source of monochromatic high energy beam of particles in an excited state.

References

1) V.V.Okorokov: Pis'ma Zh.Eksp.Teor.Fiz.2 (1965) 175.(JETP Lett.2 (1965) 111.).
2) S.Datz,C.D.Moak,O.H.Crawford,H.F.Krause,P.F.Dittner,J.Gomez del Campo J.A.Biggerstaff,P.D.Miller,P.Hvelplund,and H.Knudsen: Phys.Rev.Lett.40 (1978) 843.
3) Y.Iwata,K.Komaki,Y.Yamazaki,M.Sekiguchi,T.Hattori,T.Hasegawa,and F.Fujimoto: Nucl.Instr.Meth., to be published.
4) J.Lindhard: K.Dan.Vidensk.Selsk.Mat.Fys.Medd.34 (1965) 11.
5) O.H.Crawford and R.H.Ritchie: Phys.Rev.A20 (1979) 1848.
6) N.Neskovic: Phys.Rev.B33 (1986) 7488.
7) S.Shindo and Y.H.Ohtsuki: Phys.Rev.B14 (1976) 3929.
8) H.Nitta and S.Shindo: in preparation.
9) R.Fusina and J.C.Kimball: Nucl.Instr.Meth.Phys.Res.B33 (1988) 77.
10) V.V.Okorokov: in Proceeding of the 3rd Soviet-Japanese Symposium on Charged Particle Interactions with Solids, Tashkent,1988.

4. Ion Trap for Multiply Charged Ions

Kazuhiko Okuno

Department of Physics, Tokyo Metropolitan University

Recently, the ion trap technique has been highlighted as an useful method for very high-resolution ion spectroscopic works and very low energy collision experiments. In this paper we attempt to review some type of "Ion Trap" and their applications, and we discuss on the confinement of multiply charged ions.

1. Penning Trap and Paul(RF) Trap

The Penning trap[1] and the Paul trap[2,3] use the same configuration of two endcap electrodes and a ring electrode as shown in Fig.1. In the Penning trap, a static voltage U_0 applied between the ring and endcaps makes only a static potential well along the z-axis and the motion of charge particles can be confined by superimposing a static magnetic field along the z-axis. The Penning trap has the disadvantages of the typically strong magnetic field required and the fact that the magnetron motion is in unstable equilibrium in the trap. An important practical advantage is that parasitic heating mechanisms like RF heating in the Paul trap are nearly absent.

On the other hand, in the Paul trap, a high frequency alternative voltage $V_0\cos\omega t$, sometimes together with a static voltage U_0, are applied between the ring and endcaps. Equations of ionic motion in the Paul trap take the form of a Mathieu equations:

$$\frac{d^2X_i}{d\tau^2} + (a_i - q_i\cos 2\tau)X_i = 0$$

where $-a_z = +2a_r = 16qU_0/m\omega^2(r_0^2+2z_0^2)$

$+q_z = -2q_r = 8qV_0/m\omega^2(r_0^2+2z_0^2)$

r_0 and z_0 are the most closed distances from the center of the trap to the ring and endcap electrodes, m is the mass of ion, $\tau=\omega t/2$, and q is the charge state of ion. The region bounded by the

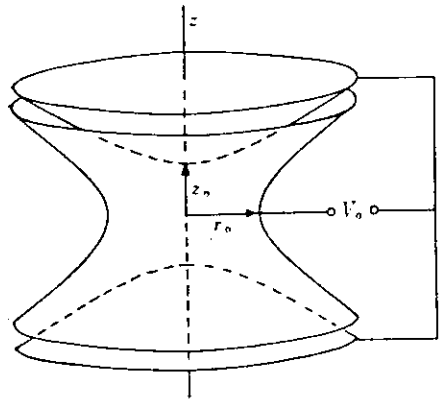

Fig.1 Electrode system for Penning trap and Paul trap.

solid line shown in Fig.2 represents the values of a_i and q_i giving stable confinement. For sufficiently high frequency ω, the ionic motion can be well approximated by that in an overall effective potential well:

$$\phi(r,z) = \left[\frac{qV_0^2}{m\omega^2(r_0^2+2z_0^2)^2} + \frac{U_0}{r_0^2+2z_0^2} \right] r^2$$

$$+ \left[\frac{qV_0^2}{m\omega^2(r_0^2+2z_0^2)^2} - \frac{U_0}{r_0^2+2z_0^2} \right] z^2$$

The trapped ions are bounded in the effective potential well in all directions with no magnetic fields. Paul trap has the capability to provide tighter confinement than the Penning trap, but the phenomenon of "RF heating" has been a limitation in some experiments. The well depth and shape of the effective potential depend on the static voltage U_0. The scanning of U_0 releases ions from the trapping region to the r or z direction and it can be used for the ion mass spectroscopy.

Optical spectroscopy using laser-induced fluorescence is a very sensitive detection method for atomic ions stored in the trap. Iffländer and Werth (1977)[4] have observed fluoresence of Ba^+ stored ions with using a dye laser system (Fig.3). The map of fluoresence yields (Fig.4) provides the relative ion storage capability of the Paul tap as function of a_z and q_z parameters.

Laser cooling, in which a monochromatic laser beam tuned slightly lower in frequency

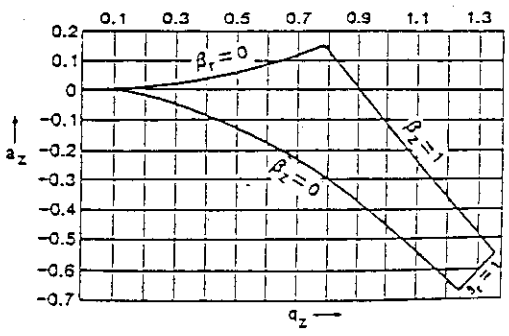

Fig.2 Theoretical stability diagram for the Paul trap.

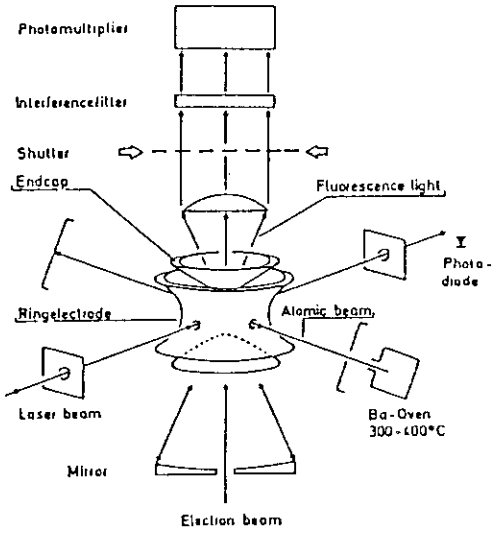

Fig.3 Observation system of fluorescence from trapped ions.

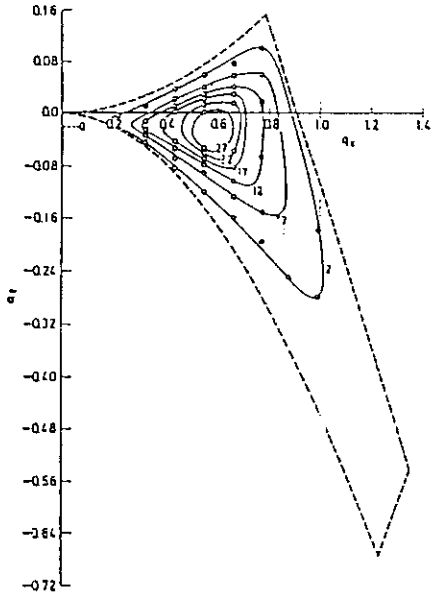

Fig.4 Relative fluorescence yields.

than a strong resonance transition is used to damp the velocity of an atom or ion, was first proposed for trapped ions by Wineland and Dehmelt (1975)[5]. This method is useful for reducing the second-order Doppler shift and first-order Doppler broadening of resonance lines. Laser cooling of stored ions has made possible to achieve a Doppler free high-resolution spectroscopy.

2. Beam Guide Technique

The beam guide technique has been pionieered by Teloy and Gerlich (1974)[6] for the study of low energy ion collisions. A full detail of the ionic motion in the multi-pole beam guide has been reported by Okuno.[7,8]

When parallel 2N multi-poles ($N \geq 2$) are equally spaced around an axis and high frequency voltages of $\pm V_0 \cos\omega t$ are supplied to them alternatively in opposite phase, the oscillatory electronic field created in the multi-pole beam guide can modulate and confine only the radial motion of charged particles and never affects the drift motion along the central axis. For sufficiently high frequency ω, the radial ionic motion in the multi-pole beam guide can be approximated by the ionic motion in an effective potential of

$$\phi(r) = \frac{(NqV_0)^2}{4m(a\omega)^2} (r/a)^{2(N-1)},$$

where m is the mass of ion, q is the charge state of ion and a is the nearest distance from the axis to electrode poles. The ion trajectory in an octo pole ion beam guide (OPIG) is computer-simulated as shown in Fig,5. The beam guide technique can store ions one-dimentionally and it is very useful for the low-energy ion beam transportation without intensity loss. Practically, Okuno has combined an OPIG with the collision cell placed at the middle of a tandem mass spectrometer and has performed multi-charged ion collision experiments in the low and wide energy region from 0.1 to 1000 eV.[7-9]

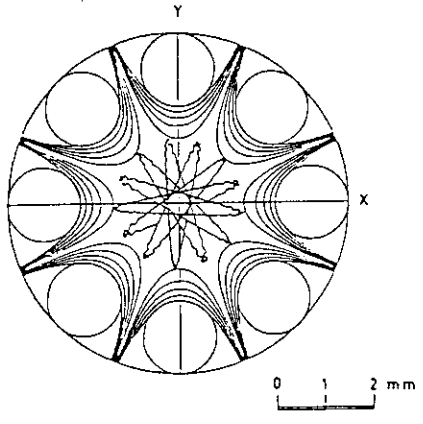

Fig.5 Cross section of OPIG and trajectory of ionic motion.

3. Electron Beam Ion Trap

The space charge trap is utilized for producing highly charged ions in the electron beam ion source (EBIS), where a high density of electron beam is prepared by the magnetic compression, the space charge of the electron beam confines ions within beam and also ions are successively ionized by the electron impact. As a typical example, mass spectra of ions extracted from a small type of "Mini-EBIS"[10] are shown in Fig.6 as a function of the ion confinement time. It is cleared that the charge distribution of extracted ions proceeds with increasing the confinement time.

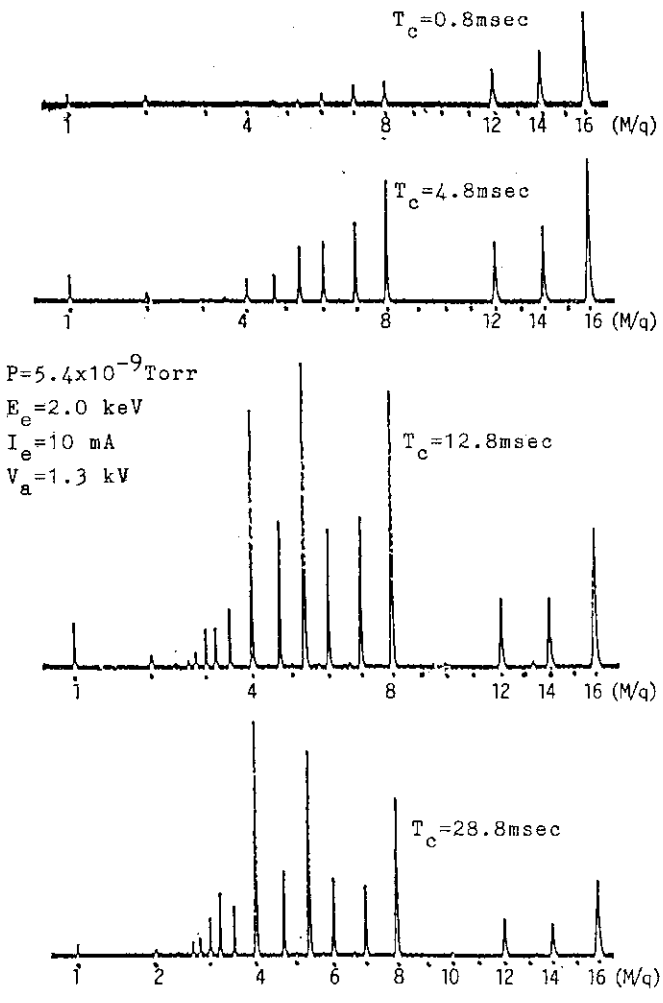

Fig.6 Mass spectra of extracted ions from Mini-EBIS as a function of confinement time T_c.

The electron beam ion trap (EBIT) based on the EBIS concept has been developed for the spectroscopic study of highly charged ions at the Lawrence Livermore National Laboratory.[11] In the EBIT, ions are trapped electrostatically instead of extracting ions as in EBIS and several features including ion cooling using light ions and plasma instability control using a short trap length are incorporated. The electron beam is used not only to trap and ionize, as in EBIS, but also to probe and excite of highly charged ions. Using the EBIT, measurements of dielectronic recombination, impact excitation, radiation polarization and radiative recombination in ion-electron collisions have been made by observing the emitted X-rays.

4. Problem in Ion Trap Study of Multiply Charged Ions

Generally, the electronic and magnetic fields supplied to create an

effective confinement potential well in ion trap become weak with decrease the M/q value of ion. Therefore, in principle, every type of ion trap mentioned above are applicable for multiply charged ions, but only EBIT has the real experience of trapping highly charged ions at present.

In order to confine multiply charged ions within the trap for long times, production of low energy multiply charged ions and ultra high vacuum condition are required. Low energy multiply charged ions can be prepared in the trap by electron impact, high energy heavy particle collision and photon (X-rays) irradiation. Successive ionization by electron impact is useful for production of highly charged ions. Recoil ions in high energy heavy particle collisions have small recoil energy but the energy tends to become large with increasing the charge state.[12] Laser cooling useful for atoms and single charged ions can not used any longer for multiply charged ions with no resonance states in the laser frequency range. Inner shell ionization by X-rays irradiation is known to have advantage for preparation of slow highly charged ions.[13] Ultra high vacuum is required to avoid influence of charge changing processes in collision of multiply charged ions with neutral particles, especially electron capture creates large translational energy even at low energy collision.[14] Ion trap studies of multiply charged ions, especially high-resolution spectroscopy and very low energy collision experiment for multiply charged ions, are in future rogram.

References

1) F. M. Penning, Physica, 3, 873 (1936).
2) E. Fisher, Z. Phys., 156, 1 (1959).
3) R. F. Wuerker, H. Shelton and R. V. Langmuir, J. Appl. Phys., 30, 342 (1959).
4) R. Iffländer and G. Werth, Opt. Commun., 21, 411 (1977).
5) D. J. Wineland and H. G. Dehmelt, Bull. Am. Phys. Soc., 20, 637 (1975).
6) E. Teloy and D. Gerlich, Chem. Phys., 4, 417 (1974).
7) K. Okuno, J. Phys. Soc. Jpn., 5, 1504 (1986).
8) K. Okuno and Y. Kaneko, Mass Spectrosc. (Janan), 34, 39 (1986).
9) K. Soejima, K. Okuno and Y. Kaneko, Abstructs of XVIth ICPEAC (New York), (1989).
10) K. Okuno, Jpn. J. Appl. Phys., 28, 98 (1989).
11) M. A. Levin, R. E. Marrs, J. R. Henderson, M. B. Schneider, Physica Scripta, T22, 157 (1988).
12) R. E. Olson, Electronic and Atomic Collisions (ed. by Gilbody et. al. 1989), p-271.
13) L. A. Sellin, J. C. Levin, C. -S. O. H. Cederquist, R. T. Short and H. Schmidt-Boecking, Physica Scripta, T22, 178 (1988).
14) For example, K. Okuno, H. Tawara, T. Iwai, Y. Kaneko, M. Kimura, N. Kobayashi, A. Matsumoto, S. Ohtani, S. Takagi and S. Tsurubuchi, Phys. Rev., A28, 127 (1983).

5. Charge Changing Collisions of ^{3}He Ions at High Energy Region

Yoichi Haruyama, *Hidemi Ogawa, **Ichiro Katayama

Laboratory of Applied Physics, Kyoto Prefectural University,
*Department of Physics, Nara Women's University,
**Research Center for Nuclear Physics, Osaka University

It requires high energies (~1 MeV and above) to investigate inner-shell processes of heavier atoms and highly charged ion processes (excitation, ionization, charge exchange and so on) in ion-atom collisions. Such energies could be obtained with tandem Van de Graaff and more powerful machines, hitherto the domain of nuclear and particle physicists. In this last decade, such machines became feasible for atomic collision research in our country. Today, there is hardly a major accelerator facility which does not have some atomic physics activity on its program. The authors have been carried out a series of experiments on inner shell electron capture of $^{3}He^{2+}$ ions by using high resolution magnetic spectrograph RAIDEN at Research Center for Nuclear Physics (RCNP), Osaka University.[1-3] We report current status of our experiments briefly.

As for the inner shell electron, its motion is largely determined by the Coulomb fields of the highly charged nuclei, it is possible to make considerable progress using models based on independent electron motion. The electron capture process in the high energy region is expected to be described by the plane wave second Born approximation. In the intermediate energy region, however, there are many approximations such as continuous distorted wave approximation, impulse approximation, strong potential born approximation and so on. In order to clarify this confusing status of theories, a high precision experimental study of the inner-shell electron capture is necessary. We have measured the energy spectrum of $^{3}He^{1+}$ ions precisely by using RAIDEN. Electron capture by ^{3}He from K shell has been measured with excellent separation from higher shells. Deconvolution calculation of the spectrum gives only the ratio of inner shell electron capture cross sections to the total ones. Total capture cross sections are indispensable for the sake of comparison with the available theoretical values.

Up to the present, due to the difficulties of preparing sufficiently

thin foil targets, measurements of charge changing cross sections of an energetic ion have been restricted to gaseous and vapor targets. The charge changing cross sections decrease with increasing energy at high energy region. There arises a chance to observe nonequilibrium charge fractions for solid targets from which one can deduce charge changing cross sections. We have measured single electron loss cross sections of $^{3}He^{1+}$ ions for various solid targets such as C, Al, V, Cr, Cu, Ge, Nb, Ag, Sn and Au at 72 MeV by using attenuation method. In this method residual $^{3}He^{1+}$ fractions after charge changing collision were measured with $^{3}He^{1+}$ incident beam. The advantages of this method are described in the following. Firstly, relatively thick targets can be used for determination of loss cross sections, compared with the growth method. For the case of a $^{3}He^{2+}$ incident beam (the growth method), equilibrium charge fractions were observed when the target exceeded about 20ug/cm^{2} in thickness while in the present method nonequilibrium fractions were observed for the targets of 50ug/cm^{2} in thickness. Secondly, simultaneous measurements of $^{3}He^{1+}$ and $^{3}He^{2+}$ yields can decrease the uncertainties in the total number of ^{3}He particles, while the growth method sometimes suffer from the uncertainties in the total charge of the incident $^{3}He^{2+}$ beam.

Thin target foils were prepared carefully by evaporating the target materials on carbon foils of 5 ug/cm^{2} in thickness. We carried out RBS and PIXE measurements to certify the thickness of the targets and their impurities by using a 2 MeV helium beam from the 4MV van de Graaff accelerator at Kyoto University, the reason being that the target thickness and impurity concentrations affect seriously the derived cross sections. It was found that there are two peaks for each oxygen and silicon atoms. Stopping power calculation shows that these contaminating atoms exist on both sides of the target surface.

Fig.1 shows the contamination corrected loss cross sections at 72 MeV as a function of target atomic number. The associated errors for the cross sections are mainly due to the counting statistics and due to uncertainties in the target thickness. Theoretical values are also shown in this figure.

With respect to the electron capture cross section, which is derived from the equilibrium charge fraction and the loss cross section, it is not simple to determine the contribution of contaminating atoms precisely. Both total and inner shell electron capture cross sections will be discussed in our coming paper.

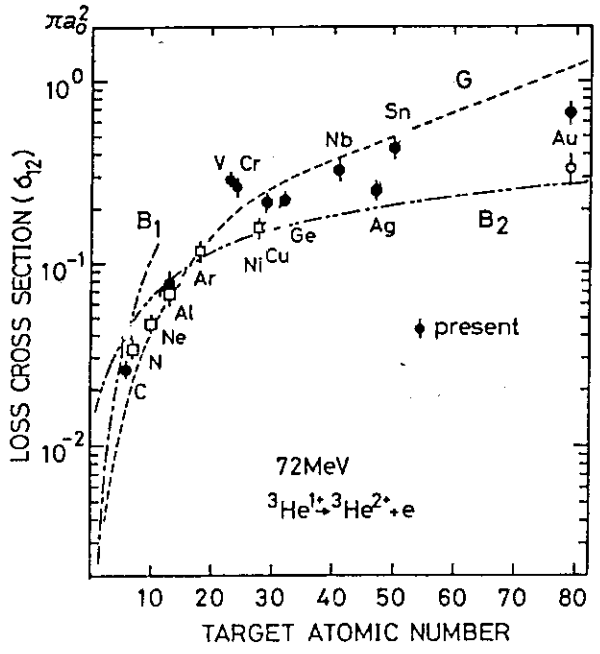

Fig.1 Target atomic number dependence of single electron loss cross sections of $^3He^{1+}$ ions at 72 MeV. Full circles denote the present results with contamination correction. Open rectangles correspond to estimated values from those measured by Katayama et al. (refs.[4-6]). Also shown are Bohr's semiclassical calculations for light (B1) and intermediate (B2) targets (ref. 7) and Gillespie's Born calculations (G) (ref.9).

References

[1] I. Katayama, M. Fujiwara, S. Morinobu, T. Noro, H.Ikegami, F.Fukuzawa and I. Sugai, Proc. 2nd Asia- Pacific Physics Conf., Bangalore, India (1986) ed. S. Chandrasekhar (World Scientific Publishing Co.Ltd.) p.622.

[2] H. Ogawa, I. Katayama, Y. Haruyama, T. Noro, H. Ikegami, F.Fukuzawa, K. Yoshida, A. Aoki and I. Sugai, Nucl. Instr. and Meth. A262 (1987) 23.

[3] Y. Haruyama, I. Katayama, H. Ogawa, T. Noro, H. Ikegami, F.Fukuzawa, K. Yoshida, A. Aoki and I. Sugai, Nucl.Instr. and Meth. B33 (1988) 220.

[4] I. Katayama, G. P. A. Berg, W. Hurlimann, S. A. Matrin, J. Meissburger. W. Oelert, M. Rogge, J.G.M Romer, J. Tain and G. Gaul, J. Phys. B17 (1984) L23.

[5] I. Katayama, G. P. A. Berg, W. Hurlimann, S. A. Matrin, J. Meissburger. W. Oelert, M. Rogge, J.G.M Romer, J. Tain and G. Gaul, Phys. Lett. 92A (1982) 385.

[6] I. Katayama, G. P. A. Berg, S. A. Matrin, J. Meissburger, W. Oelert, A. Retz, M. Rogge, J.G.M Romer, G. Gaul, H. Hasai, J. L. Tain and L. Zemlo, Z. Phys. D3 (1986) 73.

[7] N. Bohr, K. Dan. Videndk. Selsk. Mat. Fys. Medd. 18 (1948) no. 8.

[8] G. H. Gillespie, Phys. Rev. A18(1978) 1967.

6. Proposal of High Resolusion Crystal Ball

Y. Yoshizawa

Manuscript not received.

7. A High-Spin Spectrometer–the NORD BALL

Kohei Furuno

Institute of Physics, University of Tsukuba,
Tsukuba, Ibaraki 305, Japan

The NORD BALL is designed for investigations of nuclear structure at high-excitation energies and high spin by means of in-beam γ-ray spectroscopy. This new instrument has recently been installed at the Tandem Accelerator Laboratory of the Niels bohr Institute in Denmark. The project of the NORD BALL was initiated by the collaboration of four nordic countries, Denmark, Finland, Norway and Sweden.[1] Later, several other groups from Holland, Italy, Japan and West Germany participated in this project.

The NORD BALL comprises 20 Compton-suppressed germanium(Ge) γ-ray spectrometers as a basic detector. In order to achieve the highest possible sensitivity, Ge spectrometers are arranged in a close packed geometry. They are mounted on a truncated icosahedron which has 12 pentagonal surfaces and 20 hexagonal surfaces. Each Ge detector is mounted in a hexagonal surfaces.

The frame of the truncated icosahedron is set in such a way that a horizontal incident beam is injected through a pentagonal surface, and then the beam comes out towards the opposite pentagonal surface after the bombardment of the target. The 20 Compton suppressed spectrometers are positioned in four rings perpendicular to the beam axis. The polar angles θ of these spectrometers are $37°, 79°, 101°$, and $143°$, where the beam direction is taken to be $\theta = 0°$. The azimuthal angles are an integer of $72°$. Coincidences between spectrometers in a given ring with those of other rings give directional angular correlations of the observed γ rays. From the correlations, multipolarities λ and mixing ratios δ can be determined.[2]

The Ge spectrometers are Compton suppressed by a BGO scintillation detector in a coaxial symmetry with a Ge crystal.[3] The Ge detectors are of high-purity and n-type with relative efficiencies larger than 20 %. The peak-to-total ratios of the spectrometers have been measured at 1.33 MeV and an average value for all NORD BALL spectrometers is 0.55. The distance from the target to the front end of the Ge detector is 17 cm. The geometrical solid angle is about 6×10^{-3}. The total detection efficiency of approximately 1 % was obtained for experiments performed so far.

In nuclear reactions to populate highly excited and high-spin states, several channels are open, and a γ-ray spectrum contains usually some contaminants. The rejection of these unwanted γ rays, or the improvement of signal-to-noise ratio for a nuclei to be investigated can be achieved by higher folds of $\gamma - \gamma$ coincidence, a $\gamma - \gamma$ coincidence with detection of charged particles, neutrons, recoiling residual nuclei, isomers, total γ ray energy, γ-ray multiplicity and combination of these. In order to take these various mode of coincidences, BaF_2 detectors(named as "inner ball") for

γ multiplicity or sum energy measurement, a neutron wall,[4] and high-efficiency charged-particle detectors consisting of plastic scintillators[5] or silicon solid state detectors[6,7] are developed. The measurement of charged-particles and/or neutrons in coincidence with γ rays is strongly helpful to select a certain reaction channel for investigation of extremely neutron deficient nuclei far from the β stability line.

Electronics system for the NORD BALL uses conventional NIM modules in linear signal processing and ECL logic circuits to produce trigger signals, except for a few developments.

A recent technical problem is the deterioration of energy resolution in Ge detectors due to neutron radiation damage. It is reported that the deterioration grows rapidly at temperature of a Ge crystal higher than $\sim 83°K$.[8] A calculation based on a simple model for heat conduction in the cryostat suggests that the length form the end cap to the Liq. N_2 reservoir in the NORD BALL design might be too long.

In the last year, active investigations were performed on high-spin states of nuclei around $A \sim 130$. The first physics from the NORD Ball is described in ref. 9). As an important part of the NORD BALL project, the upgrading of the FN tandem accelerator of the Niels Bohr Institute has been made by connecting an rf linear postaccelerator, which can generate a total accelerating voltage of ~ 8 MV/charge. Rich high-spin spectra in a wide range of nuclei will be revealed with this NORD BALL and a ^{48}Ti beam at an energy of 225 MeV delivered by the upgraded accelerator in near future.

References

1) B. Herskind, Invited Talk given at the Second International Conf. on Nucleon-Nucleon Collisions, held at Visby, Gotland, Sweden (June 1985).
2) K.S. Krane, R.M. Steffen and R.M. Wheeler, Nucl. Data Tables **A11**, (1973) 351.
3) M. Moszynski, J.H. Bjerrgaard, J.J. Gaadhøje, B. Herskind, P. Knudsen and G. Sletten, Nucl. Instr. Meth. **A280**(1989) 73.
4) S.E. Arnell, H.A. Roth, Ö. Skeppstedt, J. Nyberg, Contribution to "6th Nordic Meeting on Nuclear Physics", Univ. of Bergen Sci/Tech. no. 208, July 4 (1989) 108
5) F. Lidén. A. Johnson, A. Kerek, A. Dafni and M. Sidi, Nucl. Instr. Meth. **273** (1988) 240.
6) S. Mitarai, Contribution to this symposium.
7) T. Morikawa, N. Kato and Y. Yoshizawa, Development at the Universities of Hiroshima and Kyushu, Japan.
8) EG & G ORTEC, private communications.
9) G.Sletten, J. Gascon and J. Nyberg, Preprint of the Tandem Accelerator Laboratory of the Niels Bohr Institute, TAL 89-3, and Proc. of the Int. Conf. on the Spectroscopy of Heavy Nuclei, 25-30 June 1989, Crete.

8. Gamma Ray Measurement by Crystal Ball in the Mass=80 Region

S. Mitarai and T. Kuroyanagi

Department of Physics, Kyushu University 33, Fukuoka 812 Japan

Si Ball consists of 12 pentagonal Si detectors with thickness of 170 μ m. Particle identification is carried out by the difference of energy loss in the Si detector. The number of the charged particles detected simultaneously is recorded on the tape in list mode.

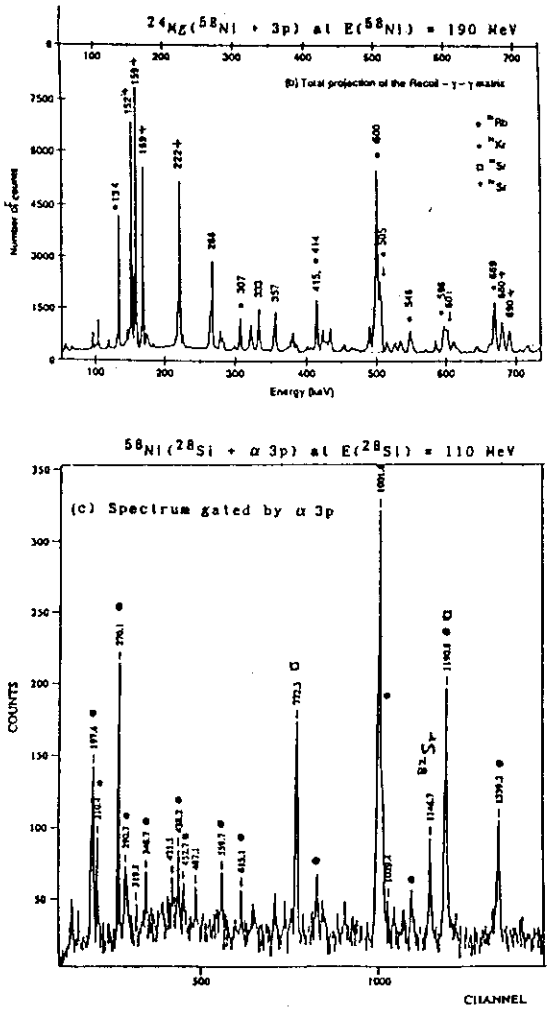

Fig.1 (a) The spectrum is projected from a matrix coincident with mass 79 recoils separated with Daresbury recil separator. (b) The α 3p gated spectrum following the (^{58}Ni + ^{28}Si) reaction.

Experiment of in-beam spectroscopy was carried out using NORDBALL and Si Ball at NBI-TAL from July 1st to 10th. The (^{58}Ni + ^{28}Si) reaction was used to study nuclei in the mass region of A = 80. Two self supporting foils of enriched ^{58}Ni of 320 μ g/cm^2 were stacked together and bombarded by the 110 MeV ^{28}Si beam from the Tandem Van de Graaff. Thickness of a target frame is 0.1 mm because of avoiding the decrease of solid angle for evaporated charged particles. Thirteen ACS Ge detectors were placed on NORDBALL framework. A Si Ball chamber of about 80 mmϕ diameter was set at the center of NORDBALL framework.

Total detectoin efficiencies of the Si Ball in this experiment are 80-85% and 65% for evaporated proton and alpha particle, respectively.

Figure 1 shows a α 3p gated

gamma spectrum in this experiment and total projection spectra of the γ -γ matrices in coincidence with mass-79 separated by a recoil mass separator in Daresbury. Data of Daresbury[1] was obtained from the $^{24}Mg(^{58}Ni,3p)^{79}Rb$ reaction at 190 MeV using an ACS Ge detector array and Recoil Separator. The transmission efficiency for residual nuclei of A = 79 are 2.0-2.5%. The spectrum in coincidence with mass-79 of charge state, q=24, contains not only lines of A = 79 nuclei (^{79}Rb and ^{79}Sr) but also weak ones of A = 76 nucleus with different charge state. A total of 0.57 million recoil -γ -γ events was accumulated, which is not so much because of low transmission efficiency of Recoil Separator. The α 3p gated spectrum in this experiment shows low continuum component and many lines of ^{79}Rb and a several lines of $^{80}Sr(\alpha\ 2p)$ and ^{82}Sr. An α 3p detection efficiency of Si Ball for ^{79}Rb is about 20% which is remarkably higher than Recoil Separator.

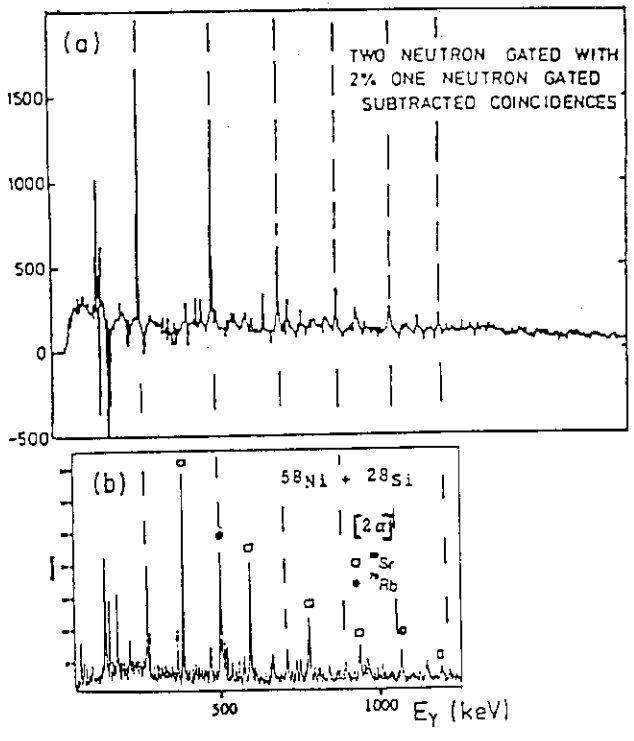

Fig.2 (a) The corrected 2n gated spectrum with 2 % of the 1n gated spectrum subtracted. (This figure is from ref. 2) (b) The 2α gated spectrum following the (^{58}Ni + ^{28}Si) reaction.

The rotational band of 78-Sr was investigated in the reaction $^{58}Ni(^{24}Mg, 2p2n)$[2] at 110MeV using POLYTESSA framework with 15 neutron detectors at forward angle and 15 ACS Ge detectors at back angle. Figure 2-a is the corrected 2n gated spectrum with 2% of 1n gated spectrum subtracted. In our experiment, nucleus of ^{78}Sr were populated in the exit channel following 2α evaporation with cross section of 1.5 mb(CASCADE calculation). Figure 2-b shows the 2α gated spectrum which shows the lines of $^{78}Sr(2\alpha)$ and $^{80}Sr(\alpha\ 2p)$. If

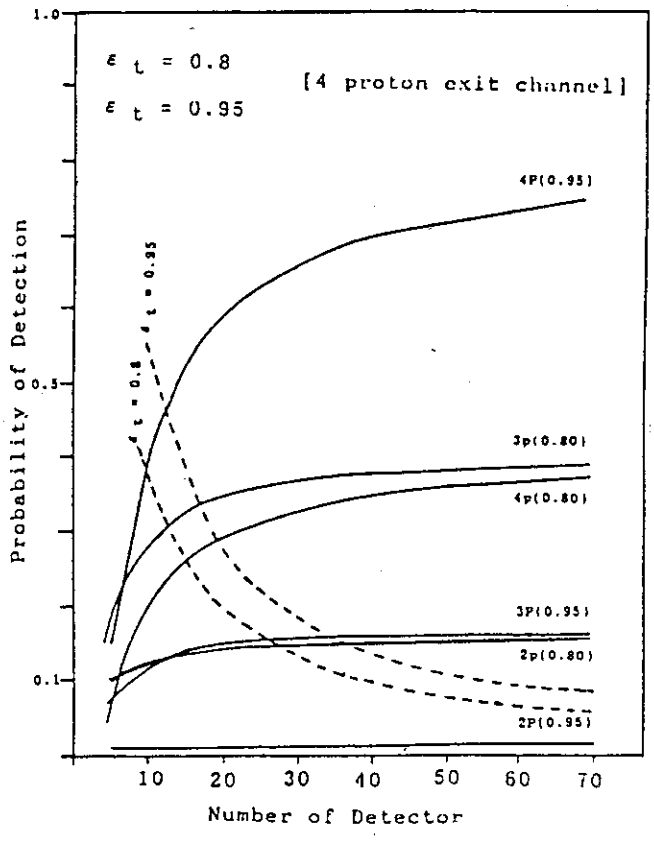

Fig.3 The probabilities of 1p, 2p, 3p and 4p detections as a function of the number of detectors in the case of 4 proton exit channel. A doted line corresponds two proton detection in one detector at a time and this probability is eliminated in the solid lines.

we had record of energy in Si Ball detectors, we could decrease the lines of ^{80}Sr by adjustment of the discrimination level between proton and alpha particle.

Calculation was carried out to obtain detection probabilities in the case of 4 proton exit channel with total detection efficiencies of 80% and 95%, which is shown in figure 3. Solid lines show the probabilities of 2p, 3p and 4p proton detections as a function of the number of detectors. The lines eliminated the detection probability of two protons on one detector at a time. A dotted line shows the probability of detection of two protons striked on one detector at a time. Those lines show that the probability of 4 proton detections (all of exit protons) increase rapidly with total detection efficiency over 80%, and a number of detectors (greater than 40 ?) are necessary to decrease the detection of two protons striked on one detector.

1) O. Skeppstedt, C. J. Lister, A. A. Chishti, B. J. Varley, W. Gelletly, U. Lens, R. Moscrop, L. Goettig, Private communication

2) C.J. Gross, J. Heese, K.P. Lieb, C.J. Lister, B.J. Varley, A.A. Chishti, J.H. McNeill and W. Gelletely, Phys. Rev. C39 (1989)1780

9. Nuclear Spectroscopy at High Spin States

Yoshifumi R. Shimizu

Department of Physics, Kyushu University, Fukuoka 812

Introduction

The new tandem booster project at JAERI is expected to open great possibilities to study detailed properties of nuclei under the influence of rapid rotations. In this report I briefly review some topics related to the nuclear spectroscopy at high spin states, which, I hope, help to develop a new research area with this new facility.

The knowledge of nuclear structure is recently extended by the high-resolution multi-detector system (crystal ball) composed of the anti-Compton suppressed arrays.[1] Above the yrast line, where the central theme is nuclear structure at finite temperature or the study of the "order to chaos" transition in nuclei, the damping mechanism of collective motions is now under intense study, for instance, the rotational damping, the decay of the giant resonances at high spin and excitation energy, and possible nuclear analogies of the "motional narrowing" phenomena.[2] On the other hand, in the region near the yrast line, it is possible to study the properties of rapidly rotating nuclei through observation of the individual quantum states and of the transitions between them. Especially, it has been now progressing to understand the mechanism of various kinds of structural change, or the "phase transition", caused by high-frequency rotations, e.g., the quasi-particle alignments, the deformation change and the collapse of pairing correlations.[3] Although both regions, above-yrast and near-yrast, are equally interesting to study, I concentrate here on the subjects of the latter region.

Selected topics on near-yrast spectroscopy

(1) Coulomb Excitation and Its Large-Scale Analysis
— detailed study of collective properties —

Coulomb excitation is known to be a clean tool to extract detailed information on the nuclear collective motions. Interesting subjects are:

1. shape degrees of freedom — static and fluctuations
2. doubly excited phonon states — β, γ and 3^- -vibrations
3. pair transfer at high spin states — manifestation of Berry phase

... etc.

As an example let me briefly mention on the first one. Combined with the high-resolution detector system and the sophisticated coupled channel calculation, it has been possible to determine a large number of nuclear matrix elements connected by the Coulomb excitation in a model independent way.[4] Then the rotational invariant observables, e.g. $(E2 \times E2)^0 = \sqrt{1/5}\, Q^2$, $((E2 \times E2)^2 \times E2)^0 = -\sqrt{2/35}\, Q^3 \cos(3\gamma)$ etc., for each individual state can be extracted by using the sum rule relations. This is a great thing: Not only the mean values (equilibrium point), $\langle Q^2 \rangle$ and $\langle \gamma \rangle$, but also the variants, $\sigma(Q^2)$ and $\sigma(\gamma)$, or the even higher skewness etc., in the conventional (β, γ)-plane can be determined experimentally.[4] This means that the potential energy surface which is a standard tool for the theoretical investigation can be checked by the experiment. Thus this type of "large-scale analysis" discriminates most severely between existing theories.

(2) Superdeformed Bands
— nuclear structure under extreme conditions —

After the first observation of the superdeformed (SD) rotational band, systematic data are now accumulating, especially in the $A \approx 150$ region.[5] Interesting subjects are:

1. mechanism of population — effect of a large splitting of GR
2. properties of the SD-band — moments of inertia
3. elementary excitations on top of it — pairing and octupole vibrations, GR's
4. mechanism of depopulation — tunneling process

... etc.

Here I would like to mention on the third point. The SD states in the $A \approx 150$ region are realized as stable configurations corresponding to the closed shell of the 2:1 deformation in exactly the same way as in the case of the fission isomers in the uranium region. However, the mechanism of stabilization is somewhat different, i.e. it is the rotational energy gain in the case of SD-bands (because of the huge moment of inertia) while it is the Coulomb energy gain in the case of fission isomers. Because of the large shell gap and the characteristic shell structure near the Fermi-level, some specific collective excitation modes are expected analogously to the case of ^{208}Pb. Theoretical investigations predict that the collective pairing[6] and octupole vibrations[7] appear in low-excitation energy region on top of the SD rotational bands, e.g. $E_x \sim 1.5-3$ MeV for pairing vibrations and $E_x \sim 2-3$ MeV for octupole vibrations in the double closed SD band of ^{152}Dy. In Fig.1 is shown the strength function for the octupole vibration at zero rotational frequency. The low-lying octupole bands, the most collective one (note that they are split into seven components by deformation and rotation) of which has signature $\alpha = 0$, i.e., it is I=even sequence if the SD "vacuum" is I=even, are especially interesting since the strong $E1$ linking transitions between them and the SD vacuum may be experimentally observable because of the mixing caused by large deformation.

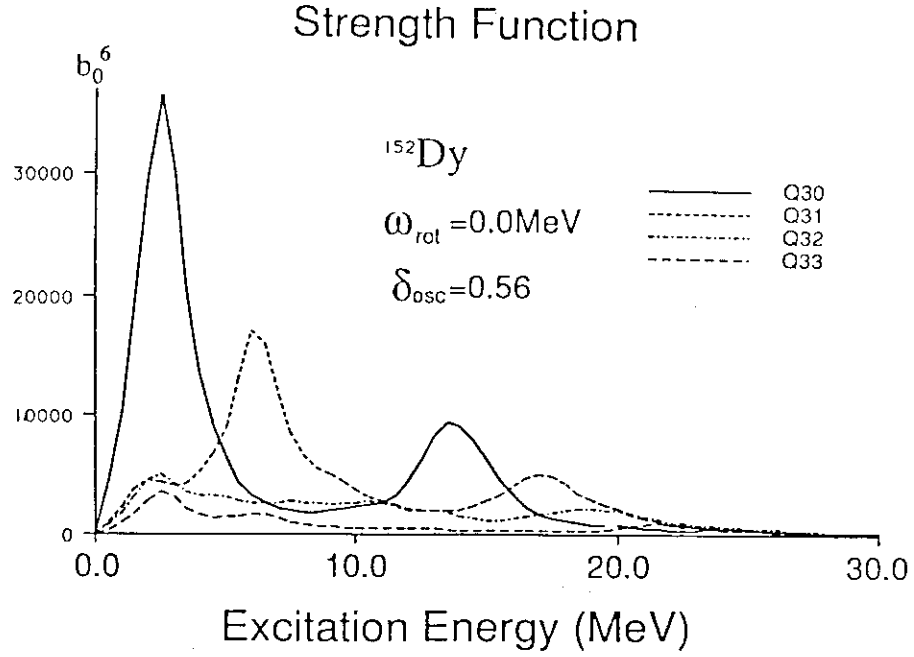

Fig. 1 The strength function for the octupole vibration excited on top of the superdeformed states in ^{152}Dy.

(3) Triaxiality and the There-Dimensional Rotation
— necessity to measure EM-transition rates —

One of the most important progress of experimental spectroscopic study made recently by the high-resolution crystal ball is that the precise measurement of the electromagnetic (EM) transition rates between high-spin rotational bands becomes possible.[1)] Interesting subjects related to this are:

1. band termination — decrease of $B(E2)_{\Delta I=2}$
2. triaxial degrees of freedom — $B(M1)$ in odd nuclei
3. nuclear wobbling motion — $B(E2)_{\Delta I=1}$ in even nuclei

... etc.

The second and third ones, which are related to each other, are mentioned here. It has been a long discussion whether the triaxial deformation is realized in actual nuclei. The point is that definite experimental information is lacking in the ground state regions. Recent experimental data of the EM transition rates indicate that the triaxial degrees of freedom in fact play an important role though it is not so definite to distinguish that they are either of static or of dynamic (vibrational) nature. A clear example of such data is the $B(M1)$ between the signature partner of the unique parity rotational bands (favoured (f) and unfavoured (u) bands) in odd nuclei: The assumption of the axial symmetry of the nuclear potential leads (through reliable theoretical models) an identity between the signature splitting of $B(M1)$ and of the routhians (excitation energy in the rotating frame), and the identity is largely violated in nuclei for which the triaxial deformation is expected from the theoretical calculations.[8)]

What is expected if the static triaxial deformation is realized at high spin states? One of the most interesting things is that a new collective motion which is closely related to the genuine three-dimensional nature of "nuclear rotor" is expected, i.e. the nuclear wobbling motion.[9)] The nuclear wobbling motion is an analogy of the excited classical motion of asymmetric top: The angular momentum vector of such a motion in the body-fixed frame precesses around the main rotation axis, the uniform rotation around which is the lowest energy motion at a given I and corresponds to the yrast states. In the near-yrast region such a precessional motion is expected to be small amplitude and a fully microscopic formulation for it is possible within the random phase approximation (RPA).[10)] In terms of the RPA the wobbling mode is described as a kind of "vibration". Actually theoretical investigations[11,12)] show that the wobbling motion strongly coupled to the shape vibrations, especially to the high-spin continuation of the γ-band, or even is expected the gradual "transition" of a RPA eigen mode excited on top of the S-band from being of the γ-vibrational nature to of the wobbling nature. Moreover, the properties of the "nuclear rotor" extracted from this microscopic calculations for the wobbling motion,[12)] for example, the three moments of inertia $\mathcal{J}_x, \mathcal{J}_y, \mathcal{J}_z$, are quite different from the macroscopic triaxial rotor model which is commonly used for the particle-rotor calculations.

Although there is no definite experimental data indicating the presence of the nuclear wobbling motion, it is extremely important to identify it in order to understand the genuine property of the "nuclear rotor". For the identification of the wobbling band, the above theoretical study suggests to look for the continuation of odd I sequence ($\alpha = 1$) of the γ-band in even-even nuclei. The essential thing is the $B(E2)_{\Delta I=+1}$ and $B(E2)_{\Delta I=-1}$ connecting the wobbling band (I=odd) and the yrast band (I=even), which will show characteristic staggering analogously to the case of

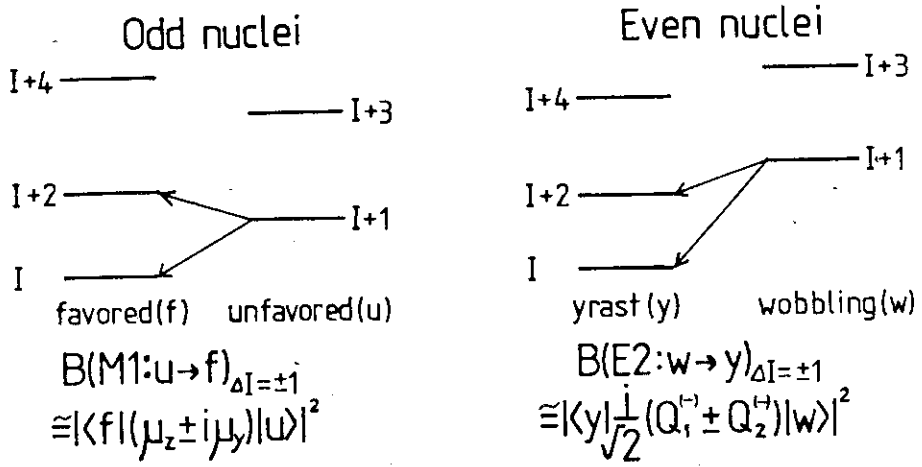

Fig. 2 An illustrative figure of the $E2$ -transition between the wobbling band and the yrast band in analogy to the $M1$ -transition between a pair of unique parity bands in odd nuclei.

$B(M1)$ of transitions between the f and u-bands (see Fig.2).

Summary

In this report I briefly reviewed some topics which I think are interesting for future study. Theoretical investigations suggest "exciting" new modes (bands), examples of which are low-lying octupole modes excited on top of the superdeformed rotational band and the nuclear wobbling motions. The identification of them is very important for deeper understanding of nuclear structure at high spin states. In order to do this it is essential to use the crystal ball type high-resolution γ-ray detector system. I hope such a device will be adopted in the new booster project at JAERI.

References

1. for example, see J. D. Garrett, G. B. Hagemann and B. Herskind, Ann. Rev. Nucl. Part. Sci. **36** (1986), 419.
2. for example, see R. A. Broglia, W. E. Ormand and M. Borromeo, Nucl. Phys. **A482** (1988), 141c.
3. for example, see J. D. Garrett et al. ed., *The Variety of Nuclear Shapes, Proc. Int. Conf. Nuclear Shape, Crete, 1987*, (World Scientific, 1988).
4. D. Cline, Ann. Rev. Nucl. Part. Sci. **36** (1986), 683.
5. for example, see M. A. Deleplanque et. al., Rev. Rev. **C39** (1989), 1651.
6. Y. R. Shimizu, E. Vigezzi and R. A. Broglia, Phys. Lett. **198B** (1987), 33.
7. S. Mizutori, Y. R. Shimizu, K. Matsuyanagi, KUNS-Preprint, Nov., 1989
8. for example, see G. B. Hagemann and I. Hamamoto, Phys. Rev. **C** to be published.
9. Å. Bohr and B. R. Mottelson, *Nuclear Structure*, Vol. II, (Benjamin, New York, 1975)
10. E. R. Marshalek, Nucl. Phys. **A331** (1979), 429.
11. Y. R. Shimizu and K. Matsuyanagi, Prog. Theor. Phys. **70** (1983), 144; **72** (1984), 799.
12. M. Matsuzaki, Nucl. Phys. **A** to be published.

10. HFB Calculation of Blocking State - Nuclear Structures of High Spin States of Odd and Odd-odd Nuclei

T. Tanabe

Manuscript not received.

11. Low Temperature Nuclear Orientation

Susumu Ohya

Department of Physics, Niigata University

The aim of this brief review is to give an outline of low temperature nuclear orientation (LTNO) and nuclear magnetic resonance on oriented nuclei (NMR-ON). When a nucleus with spin I_0 and magnetic moment μ is subject to a magnetic field B, the 2I + 1 energy levels will be split by an amount $\mu B/I_0$. By a sufficiently low temperature and a high magnetic field ($\mu B/I_0 kT \gtrsim 1$) the nuclei will be polarized along the direction of the applied magnetic field, and the population of nuclear energy levels becomes unequal. If we use a hyperfine field in a ferromagnetic host metal (for example, the magnetic field of CoFe is 290 kG), we have to cool down to 10 mK. Commercially available refrigerators achieve continuously maintained temperature down to about 5mk.

From the measurement of a temperature dependence of angular distribution $W(\theta)$, the magnetic moment can be determined. Fig. 1 shows the example for the ground state (1^+) of ^{106}RhFe.[1] The solid lines represent least squares fits to the data. The hyperfine field of RhFe is well known to be -556.6 (12) kG. From these analyses the magnetic moment was determined to be $|2.52(5)|\mu_N$.

NMR-ON is an extension of the basis LTNO measurement in which, after the nuclear ensemble has been oriented to produce observable anisotropy, a radiofrequency (RF) field is applied along an axis perpendicular to the axis of orientation. When the RF frequency equals the hyperfine splitting, i.e $h\nu = E_M - E_{M\pm1}$, the population of the linked levels tend to equalise, and the effect influences directly the observed γ ray counting rates. Thus the angular distribution of radiation is used as a detector of NMR. The value of this extension of the method is that the hyperfine splitting can be determined with a precision of 1 in 10^3 or better. Recent studies on heavy impurities such as Ir and Au embedded in cubic ferromagnetic hosts revealed the existence of a small electric field gradient resulting from an unquenched oriental momentum in addition to a large magnetic hyperfine field. Using this method, not only magnetic moments but also quadruple moments have been measured in Ir and Au isotopes. Fig. 2 shows the resonance spectra of ^{196}AuFe[2] As this NMR-ON method provides accurate values of the magnetic hyperfine splitting, it gives us the information concerning the impurity environments such as small electric

field gradient, concentration effects and vacancies. Many of these subjects are treated in a complete review by Stone and Postoma.[3]

The low temperature nuclear orientation has been a very productive experimental technique for studying nuclear structure from radioactive decays. Since about 1980, the combination of an on-line isotope separator and dilution refrigerator has reduced half life limit of the radioisotope from several hours to several seconds. Such an on-line nuclear orientation facility has made it possible to apply low temperature nuclear orientation to a wide range of short-line nuclei far from stability. The on-line facilities exist now in Lueven, Daresbury, CERN, and Oak Ridge. A recent review of on-line nuclear orientation is given by Stone and Rikovska.[4] We hope to construct such a facility in Japan.

References

1) S. Ohya, C. J. Ashoworth, Z. Nawaz, N. J. Stone and P.J. Back, to be published in Phys., C (1990) in press.
2) S. Ohya, S. Ohtake, K. Nishimura and N. Mutsuro, Phys. Rev. C36 (1987) 2072
3) Low Temperature Nuclear Orientation, eds. N. J. Stone and H. Postma (North-Holland, Amsterdam, 1986)
4) Proceeding of the first international Conference on On-line nuclear orientation, eds. N. J. Stone and J. Rikovska, Hyp. Int. 43 (1988).

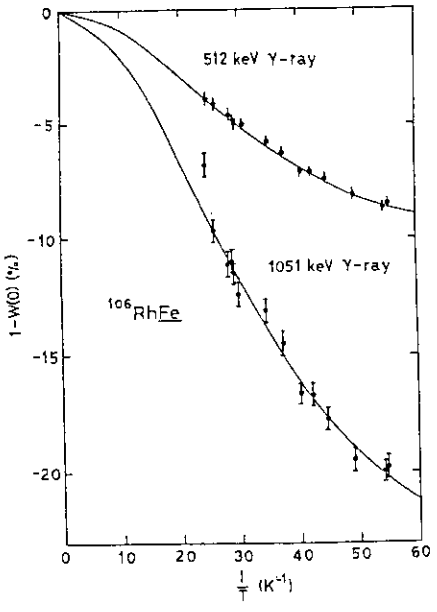

Fig. 1 1-W(θ) vs 1/T for ^{106}RhFe.

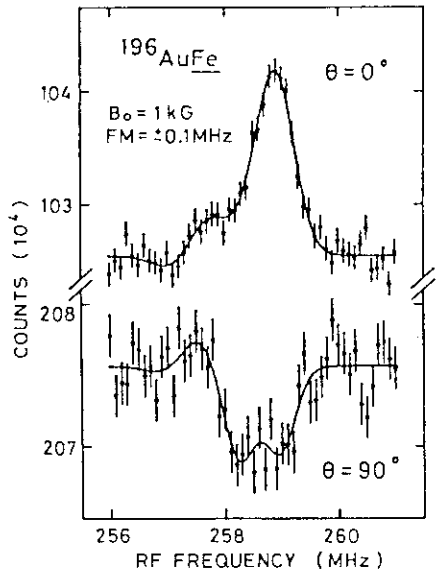

Fig. 2 NMR-ON for ^{196}AuFe.

12. Method of Laser Ion Trap

T. Shinozuka

Manuscript not received.

13. Test of IBM Prediction of Band Structure of Heavy Nuclei

Takaharu Otsuka

Department of Physics, University of Tokyo, Hongo, Bunkyo-ku, Tokyo, Japan

§1. Introduction

This talk consists of topics;

(1) M1 transition and proton-neutron symmetry in collective states
(2) β_m band
(3) super β and super γ bands in actinide nuclei
(4) signature dependence in odd-A nuclei and IBFM

The topics (2), (3) and (4) are reported in Refs. [1], [2] and [3], respectively. Because of this and the length limitation, I shall focus on the topic (1) in the following.

§2. M1 transition in the IBM-2

We have proton bosons, s_π and d_π, and neutron bosons, s_ν and d_ν in the Interacting Boson Model - 2 (IBM-2) [4,5]. The proton-neutron symmetry in IBM-2 is described in terms of F-spin [4,5]. The F-spin is similar to the isospin for nucleons; a proton boson carries F=1/2 and F_z=1/2, while a neutron boson F=1/2 and F_z=-1/2. The F-spin obeys the algebra of the angular momentum as the isospin does. The F-spin value of the states with N_π proton bosons and N_ν neutron bosons can range from F=$(N_\pi + N_\nu)/2$ to F=$|N_\pi - N_\nu|/2$. The F-spin raising operator F_+ transforms a neutron boson to the corresponding proton boson, and the F-spin lowering operator does the opposite.

The standard IBM-2 Hamiltonian is written as

$$H = \epsilon \times n_d - \kappa(Q_\pi \cdot Q_\nu) + M \qquad (1)$$

where ϵ is the single d-boson energy relative to the s boson, n_d is the d-boson number operator, κ is a coupling constant, $Q_{\pi(\nu)}$ denotes the proton (neutron) boson quadrupole operator. The quadrupole interaction in this Hamiltonian is attractive ($\kappa > 0$), and favors the states of the maximum F-spin value (called totally symmetric state). Although the realistic Hamiltonian is not invariant with F-spin, it conserves the F-spin to a large extent for low-lying states. The states of lower F-spin values are referred to as mixed-symmetry states. The states dominated by mixed-symmetry components appear at relatively higher energies. Their excitation energies are controlled by the Majorana interaction M in eq. (1).

The M1 operator in IBM-2 is written as

$$T^{(M1)} = g_\pi L_\pi + g_\nu L_\nu \tag{2}$$

where the g's are boson g-factors, and the L's denote the proton and neutron boson angular momentum operators. The usual values of the g's are $g_\pi \sim 1$ and $g_\nu \sim 0$. Eq. (2) is rewritten as

$$T^{(M1)} = \frac{1}{2}(g_\pi + g_\nu)(L_\pi + L_\nu) + \frac{1}{2}(g_\pi - g_\nu)(L_\pi - L_\nu) \tag{3}$$

The first term on the right hand side (RHS) of this equation is an F-scalar operator, and is proportional to the total angular momentum operator. It contributes only to the magnetic moment, producing no M1 transition. The second term is F-vector, and is able to change the F-spin by one. Although it can cause M1 transitions in general, its off-diagonal matrix element is vanished between totally symmetric states. Thus, the M1 transition is completely forbidden between totally symmetric states.

In practical IBM-2 calculations with the Hamiltonian in eq. (1), the F-spin is conserved to a large extent. Because of forbidden M1 transition between totally symmetric states, the M1 transition can be a good tool to see the F-spin breaking in low-lying states.

§3. Recent experiment for ^{130}Ce

Recently, some branching ratios have been measured in JAERI by Sekine *et al.* for ^{130}Ce and other neighboring nuclei. Puddu *et al.* [6] carried out an IBM-2 calculation about ten years prior to this experiment. The measured experimental excitation energies and branching ratios agree very well with this IBM-2 prediction [7], suggesting the validity of the IBM-2 in this region.

Branching ratios with $\mid \Delta J \mid \leq 1$ contain M1 components, which are sensitive to the F-spin breaking as discussed above. The F-spin breaking depends on the Majorana interaction in eq. (1). The Majorana interaction consists of

$$M = \Sigma_{L=1\ \&\ 3}\, \xi_L([d_\pi^\dagger d_\nu^\dagger]^{(L)} \cdot ([\tilde{d}_\pi \tilde{d}_\nu]^{(L)}) + \xi_2 \frac{1}{2}((d_\pi^\dagger s_\nu^\dagger + s_\pi^\dagger d_\nu^\dagger) \cdot (\tilde{d}_\pi s_\nu + s_\pi \tilde{d}_\nu)) \tag{4}$$

where the ξ's are strength parameters. Five sets of the values of the ξ's, denoted as sets A $\sim$ E, are considered (see Table 1).

In Figs. 1 and 2, branching ratios are shown for the sets A $\sim$ E, and are compared with the experimental data of Sekine *et al.* It is clear that neither set A nor B can explain experiment. The former is the case with no Majorana interaction, while the latter is equivalent to IBM-1. The sets C and D are able to describe the data. Thus, the branching ratio can exclude some cases.

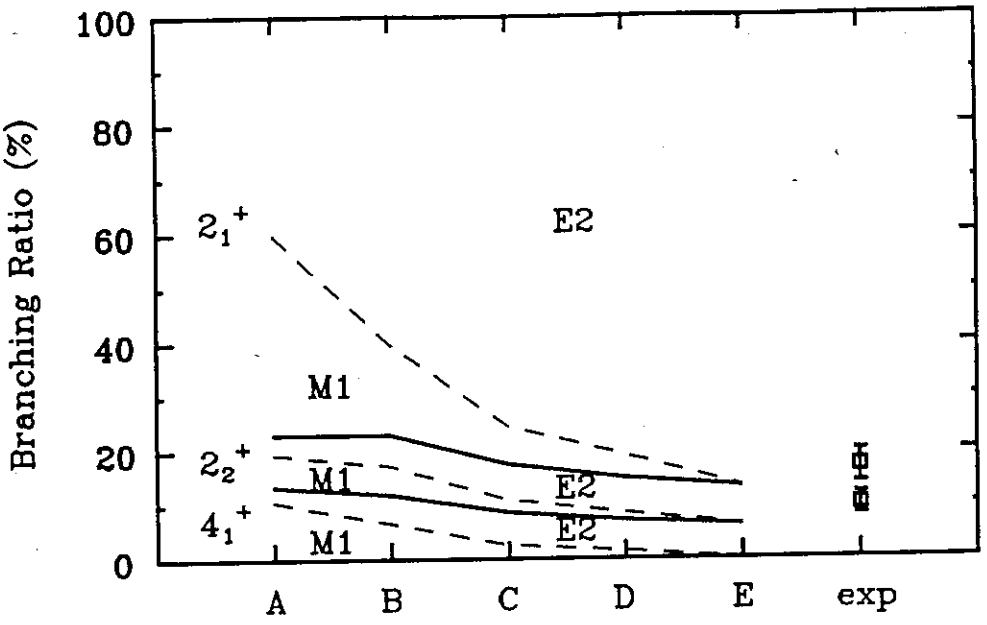

Fig 1 Branching ratios from the 3_1^+ state to the 2_1^+, 2_2^+ and 4_1^+ states of ^{130}Ce. The solid lines are calculations with the Majorana parameter sets A ~ E (see Table 1), while the points are experiment ("exp"). The E2 and M1 components are devided by dashed lines.

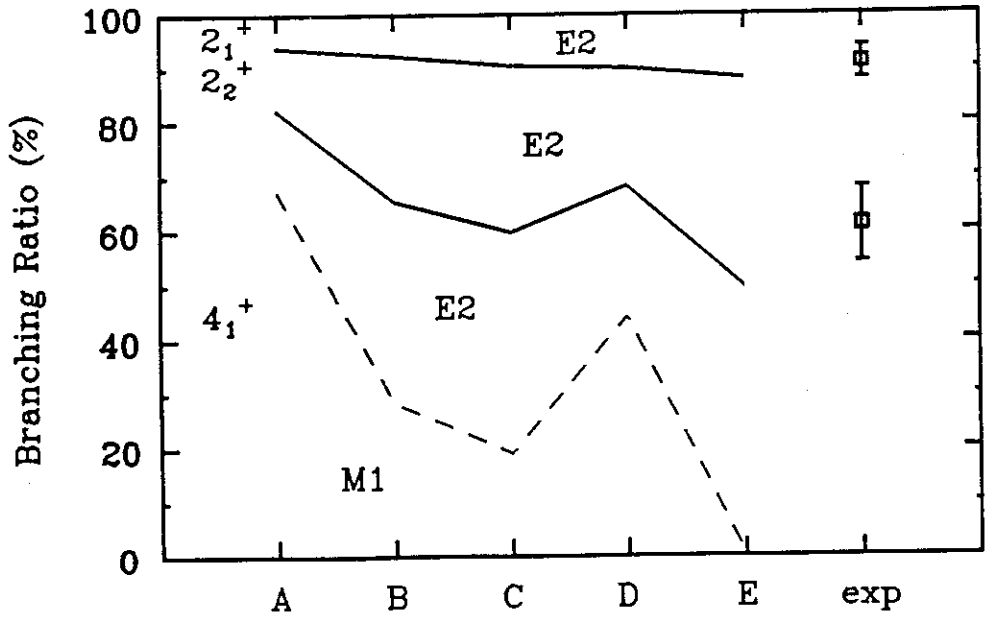

Fig 2 Branching ratios from the 4_2^+ state to the 2_1^+, 2_2^+ and 4_1^+ states of ^{130}Ce. See the caption of Fig. 1.

Table 1 Value of the Majorana parameters (MeV)

set	A	B	C	D	E
ξ_1	0.0	0.24	0.24	1.0	∞
ξ_2	0.0	0.24	0.24	0.0	∞
ξ_3	0.0	-0.18	0.24	1.0	∞

Figs. 1 and 2 show also E2 and M1 components. Although the sets C and D produce similar values of the branching ratios, the E2 and M1 components are different appreciably. The E2 transition matrix elements are insensitive to the Majorana interaction. Their variation in Figs. 1 and 2 is predominantly due to the change of the normalization factor which involves the M1 transitions. One finds that the M1 component decreases basically as the Majorana interaction becomes more repulsive, but depends also on the type of the Majorana interaction. This is quite clear in comparison between the sets C and D. Note that the excitation energies of the states in Figs. 1 and 2 are rather insensitive to the Majorana interaction, because totally symmetric components are dominant in these states.

The E2 and M1 components have not been measured separately for these nuclei. It is desired strongly that such measurement will be carried out in the near future, because no experiment has suggested what type of Majorana interaction should be used. Such information should provide us with a new insight of the proton-neutron symmetry in collective states.

References

[1] O. Scholten *et al.*, Phys. Rev. **C32** (1985) 1729.

[2] T. Otsuka and M. Sugita, J. Phys. Soc. Japan **58** (1989) Suppl. p. 530.

[3] N. Yoshida *et al.*, Nucl. Phys. **A503** (1989) 90.

[4] T. Otsuka *et al.*, Phys. Lett. **76B** (1978) 139.

[5] T. Otsuka *et al.*, Nucl. Phys. **A309** (1978) 1.

[6] G. Puddu *et al.*, Nucl. Phys. **A348** (1980) 109.

[7] T. Sekine *et al.*, JHP-Supplement (Institute of Nuclear Study, University of Tokyo, March, 1989), **3**, p. 75.

14. Effects of γ-vibration on Signature-dependence of Energy Spectra and Electromagnetic Transitions of Unique-parity Rotational Bands

Takafumi Shimano and Akitsu Ikeda

Department of Physics, Tokyo Institute of Technology,

Oh-okayama, Meguro, Tokyo 152, Japan

The quadrupole deformaton is the most important in nuclear deformations. If a nucleus has a quadrupole deformation, the whole system is invariant under the rotation by 180° around a principal axis of the deformation. Associated with this invariance we can introduce a quantum number called signature. For rotational bands in odd-A nuclei the signature quantum number is defined as $\alpha_I = \frac{1}{2}(-1)^{I-1/2}$. The signature quantum number is closely related to the following two features of unique-parity rotational bands of odd-A nuclei.

(1) The states in the band with spin $I = j +$ even are shifted downwards in energy relative to the states with $I = j +$odd, where j denotes the spin of unique-parity orbital. The former and the latter bands are called favored and unfavored band, respectively.

(2) The $B(M1; I \rightarrow I-1)$ values for the tansition from favored band to unfavored band are larger than the ones from unfavored band to favored band.

Experimental and theoretical studies have established that these two features come from the coupling between particles and nuclear rotation (the Coriolis coupling). From recent experiments, however, it is known that some nuclei show the feature which is contrary to the well established feature (1). In the unique-parity S-bands of ^{155,157}Ho,[1),2)] ^{159}Tm,[3),4)] ^{161,163,165}Lu,[5)−7)] unfavored band is favored in energy than favored band over a wide spin range. We call this remarkable phenomenon as the signature inversion.

In order to explain this phenomenon, we have proposed the particle-plus-rotor model which takes into account the γ-vibrational degrees of freedom [8)]. In our model, a nuclear system has an axial symmetric equilibrium deformation and degrees of freedom of axial symmetry breaking. When the system undergoes γ-vibration, this symmetry is broken, and the rotation axis wobbles relative to the mass distribution of the core (rotation-vibration coupling), and particles feel an axial asymmetric average field (particle-vibration coupling). These two couplings are important effects originating from the introduction of γ-vibration [9)].

We have found that our model can reproduce the signature inversion very well in the above mentioned nuclei. In Fig.1 we show the energy spectra of ^{157}Ho and ^{159}Tm, as an example, in the form of $\Theta_I \equiv (E_I - E_{I-1})/2I$, which is a convenient way to show the signature-dependence of the spectra clearly.

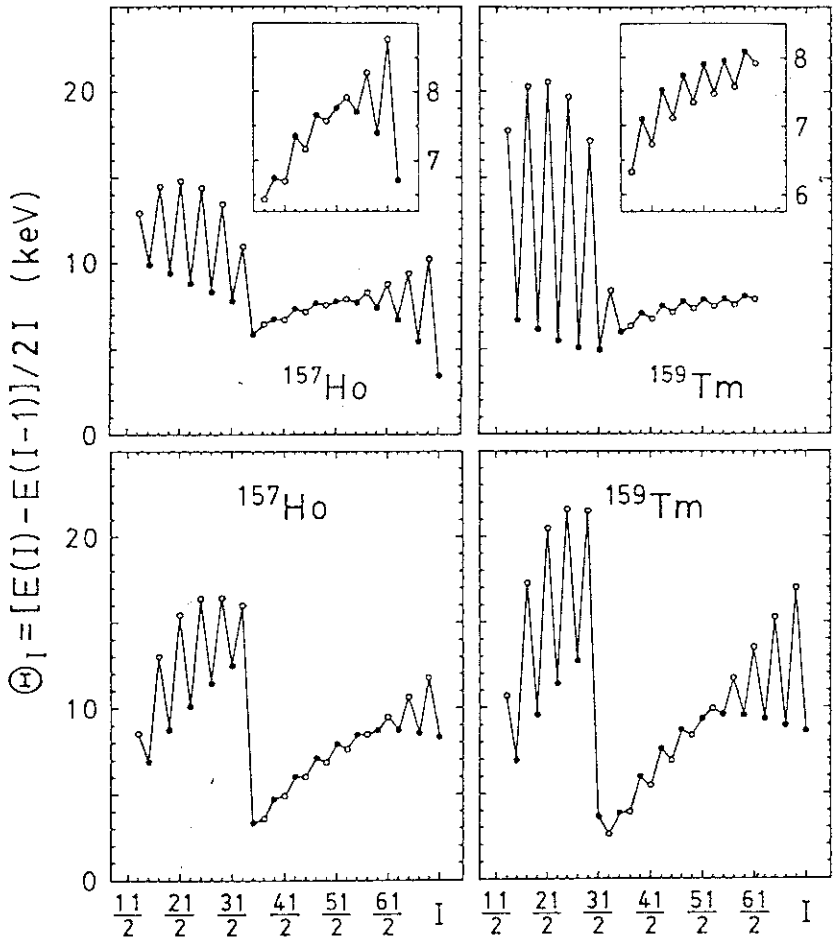

Fig.1 The experimental (upper part) and theoretical (lower part) energy spectra of the $h_{11/2}$ bands of ^{157}Ho and ^{159}Tm in the form of Θ_I vs. I. Filled (open) circles represent Θ_I for $I = j +$even(odd). Experimental data are taken from refs. 2,10 and 3.

In order to reproduce the signature inversion in the present model, it is essential to assume specific dependence of the moments of inertia on triaxial deformation γ. This γ-dependence of the moments of inertia appears in the relative phase between rotation-vibration coupling and particle-vibration one. If the moment of inertia around the shortest axis is the largest, our model reproduces the signature inversion phenomenon. If we use the well known moments of inertia of the irrotational flow model in which the one around the axis of intermediate length is the largest, the normal signature-dependence is enhanced and the phenomenon is never reproduced.

Using the wave functions obtained, we have calculated the M1 transition strengths. We show the $B(M1; I \to I-1)/B(E2; I \to I-2)$ of ^{157}Ho and ^{159}Tm in Fig.2 . The experimental data of $B(M1)/B(E2)$ of ^{157}Ho are taken from ref. 10. These are the most reliable data at present. These data show that the signature-dependence of $B(M1)$ is normal in the region of the signature inversion in energy. Our results reproduces the feature of the $B(M1)$ quite well.

Theoretical results of the energy spectra, M1 and E2 transition strength for other nuclei will be published elsewhere.

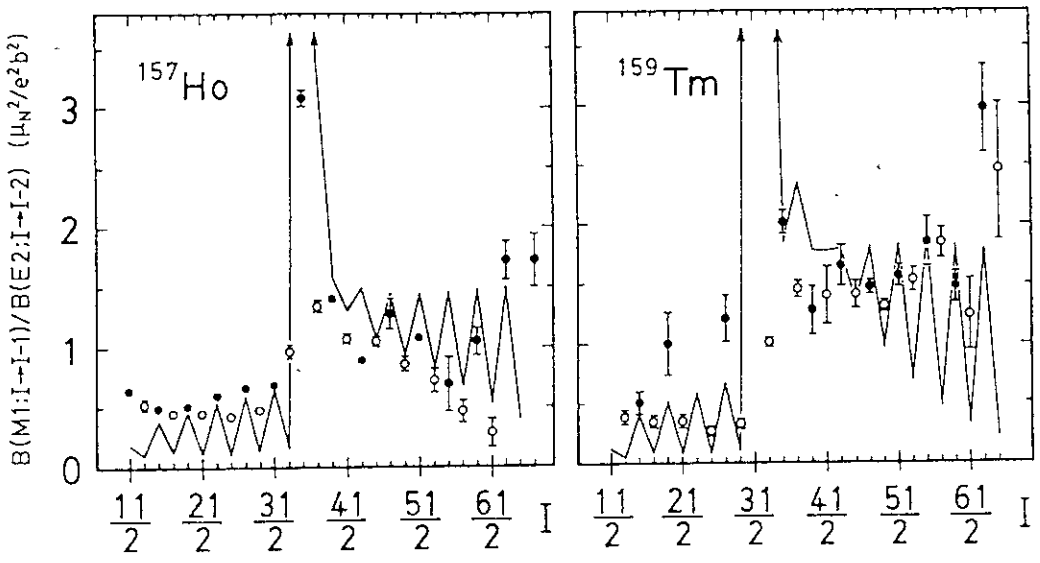

Fig.2 The experimental (circles) and theoretical (solid lines) $B(M1; I \rightarrow I-1)/B(E2; I \rightarrow I-2)$ of the $h_{11/2}$ bands of ^{157}Ho and ^{159}Tm. Experimental data are taken from refs. 10 and 11.

References

1) G. B. Hagemann *et al.*: Nucl. Phys. **A424** (1984) 365.

2) J. Simpson *et al.*: Phys. Rev. Lett. **54** (1985) 1132, and references therein.

3) R. Holzmann *et al.*: Phys. Rev. **C31** (1985) 421, and references therein.

4) J. Gascon *et al.*: Nucl. Phys. **A467** (1987) 539, and references therein.

5) C. -H. Yu *et al.*: Nucl. Phys. **A489** (1988) 477.

6) K. Honkanen *et al.*: American Chemical Society Symposium Series No.324, *Nuclei Off the Line of Stability* 1986 ed. R. A. Meyer and D. S. Brenner, p.555.

7) P. Frandsen *et al.*: Nucl. Phys. **A489** (1988) 508, and references therein.

8) A. Ikeda and T. Shimano: Phys. Rev. Lett. **63** (1989) 139.

9) A. Ikeda: Nucl. Phys. **A439** (1985) 317.

10) D. C. Radford *et al.*: Workshop on Nuclear Structure, slide report, May 16-20,1988, The Niels Bohr Institute, p.124.

11) J. Simpson *et al.*: in Proc. Int. Nuclear Physics Conference, Harrogate, U. K., Aug. 1986, vol.1, p.B66.

15. Some Facets of Low Energy Heavy-Ion Collisions - Fusion, Decay of a Compound Nucleus
N. Takigawa

Manuscript not received.

16. Cooling Processes of Hot Nuclei

Yasuhisa Abe

Research Institute for Fundamental Physics, Kyoto University

Some interesting aspects in decays of hot nuclei are discussed. The first is one in the framework with the thermal equilibrium assumed, and the second is effects due to a possible non-equilibrium process. i) Multifragmentation may start from unexpectedly low excitation energies. This casts a doubt on usual estimations of initial excitation energy by neutron multiplicity with the assumption of sequential evaporations. ii) The other interesting aspect is concerning effects of transient in fissioning mode and other collective modes of hot nuclei, which give rise to an additional influence on neutron multiplicity etc..

Many frameworks have been invented to treat multifragmentation processes. One of them is an extension of Bohr-Wheeler theory of nuclear fission to multifragmentation.[1] There one has to look for a saddle point in multifragment configuration space and an outward current at the point. Actually one has to look for minimum current, because the current is to be minimum at saddle point along decay path.

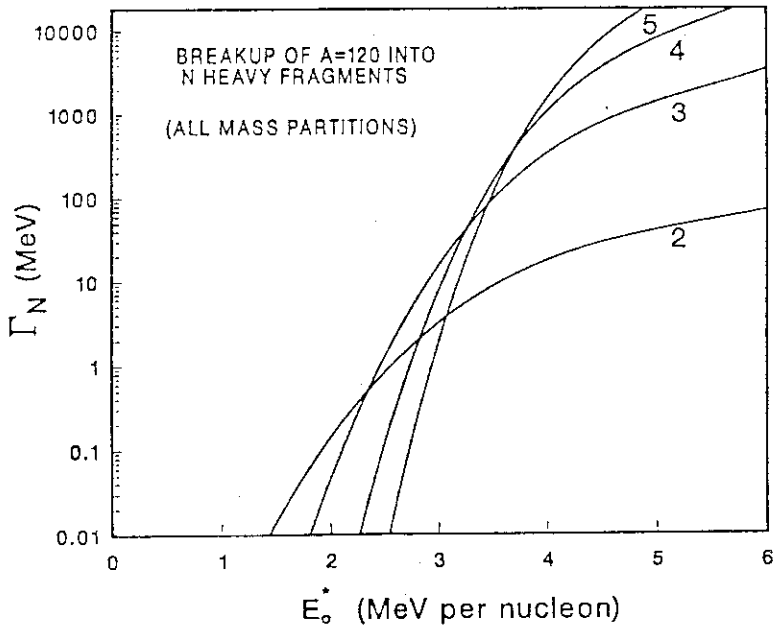

Fig.1 Partial width $\Gamma_N(E)$ for breakup into N prefragments with mass numbers $A > 10$. The curves are labelled by the value of N.

In Fig.1 partial width Γ_N for decay into N fragments is shown as a function of

the excitation energy per nucleon E_0^* of the compound nucleus with $A = 120$. It is surprising that at a little higher than 2 MeV/nucleon three body decays start to be predominant over two body decays. Another framework is a phase space approach, which should be consistent with Weisskopf theory for evaporation and with the above theory for multifragmentation in low excitation energies. The essential assumption is that the decay probability should be proportional to the state density of the relevant channel. So-called freeze-out volume inevitably comes into as a parameter. The final state density d_k can be expressed by the product of the amount of the phase space ρ_k for k free particles in the freeze-out volume V, and the level density of excited fragments ω.

$$d_k = \int_0^{E-\sum_j kj\cdot Q_j-\sum_j kj\cdot V_j} \omega(E_k)\cdot\rho_k(E-\sum_j kj\cdot Q_j - E_k)\,dE_k \qquad (1)$$

, where V_j denotes the barrier height between j-particle and the residual nucleus. The minimum kinetic energy to escape from the residual nucleus is assumed to be $\sum_j k_j \cdot V_j$. j denotes species of particle emitted (for example, $j = 1, 2, 3\ldots$.correspond to $n, p, d, \ldots$) and k_j the multiplicity of j-particle, being $\sum_j k_j = k$. With this framework, one can calculate "multiparticle evaporation" as well as usual evaporation process, by suitably choosing the freeze-out volume. Preliminary results also show that multiparticle evaporations start to be appreciable from rather low excitation energies. An interesting consequence immediately coming up is a difference in cooling process. An energy loss per neutron, for example, is different from $2\cdot T+Q$ for usual evaporation by Weisskopf theory, where T is a nuclear temperature and Q the Q-value for neutron emission. The repetition of the process gives rise to a different cooling path from the sequential evaporation. We, therefore, should take into account multiparticle emissions in estimations of the initial excitation energy of the compound nucleus from neutron multiplicities. A possible maximum energy which can be deposited in the nucleus will be modified.

Anomalous neutron multiplicities measured in coincidence with fission have forced us to re-examine fission dynamics, though the above process also should be taken into account. The fission probability is believed to be accurately given by Bohr-Wheeler theory. As is well known, Bohr-Wheeler's expression for fission width corresponds to Kramer's stationary limit of decay rate obtained by Fokker-Planck equation. This indicates that fission decay width is not constant, but is time-dependent and reaches Bohr-Wheeler value after some transient period.[3] The underlying physical picture is, roughly speaking, a slowly-moving fissioning-mode approaching to the thermal equilibrium with many degrees of freedom of rapidly moving nucleons. The fissioning-mode is considered as a Brownian particle, which therefore obeys the diffusion equation. During

the transient time or dead time for fission, neutrons can evaporate, which give rise to extra multiplicities compared to ones obtained in the stationary regime, i.e., in usual statistical model. Actually one can obtain the time-dependent decay rate by solving Fokker-Planck equation.

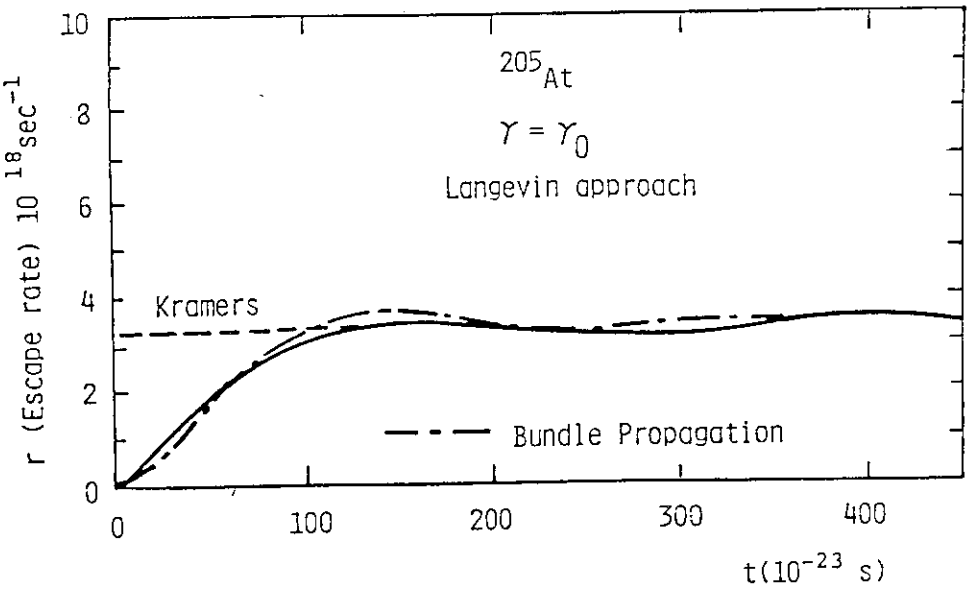

Fig.2 The time dependent decay rate $r = \Gamma_f(t)/\hbar$ is shown. $\gamma = \gamma_0$ corresponds to the unit reduced friction.

In Fig.2 examples are shown for ^{205}At, the dot-dashed curve being an approximate solution of Fokker-Planck equation and the solid curve being a solution of the equivalent Langevin equation .[4] One can see the existence of the transient time at the beginning and after that, decay rates approach to Kramers' limit (dashed line). Dynamical evolutions of hot nuclei including the time-dependent fissioning-mode and particle evaporations can be treated by the generalized Fokker-Planck equation which takes into account the coupling of the master equation describing particle evaporations.[5]

An example of the results on neutron multiplicities is shown in Fig.3, where those obtained by the dynamical treatment are approximately twice as large as those by the conventional statistical model. The existence of the transient time has not yet been established completely. Many experimental and theoretical efforts are now being continued.[6] Recently multiplicities of intermediate mass fragments have been measured, which again appear to show up effects due to the transient time.[7]

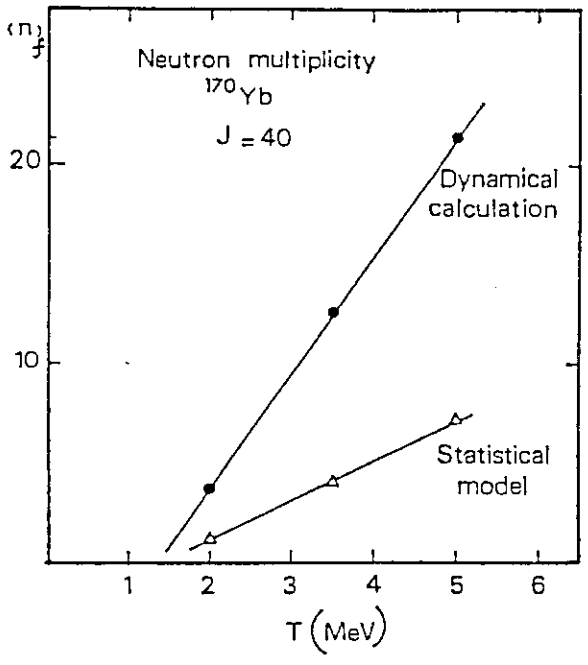

Fig.3 Neutron multiplicities are shown as functions of the nuclear temperature for ^{170}Yb with spin $J = 40$.

In summary, dynamics of hot nuclei is a new field to explore and provides a physical entity with which we can study dynamical equilibration processes of various degrees of freedom in finite quantum systems.

References

1) J.A. Lopez and J. Randrup, Nucl. Phys. **A503** (1989) 183.

2) M. Ohta and Y. Abe, under preparation.

3) P. Grangé, Li Jun-Qing and H.A. Weidenmueller, Phys. Rev. **C27** (1983) 2063.

4) Y. Abe, C. Grégoire and H. Delagrange, J. de Physique no.8, Tome **47** (1986), C4-329.

5) H. Delagrange, C. Grégoire, F. Scheuter and Y. Abe, Z. Phys. **A323** (1986) 437.

6) D.J. Hinde, D. Hilscher and H. Rossner, Nucl. Phys. **A502** (1989) 497c

7) J. Pochodzalla, R.J. Charity, U. Lynen, H. Sann, W. Trautmann and R. Trockel, preprint GSI-89-68, Sept. 1989.

17. Evolution of the Heavy-Ion Reaction −Mechanism from Fusion to Multi-fragmentation −

Toshiki Maruyama, Akira Ohnishi and Hisashi Horiuchi

Department of Physics, Kyoto University, Kyoto 606

The microscopic model which is dubbed quantum molecular dynamics (QMD) by Aichelin and Stöcker has been devised and developed as one of the numerical simulation methods to study medium and high energy heavy-ion reactions.[1,2] The simulation approach[3] by Boal and his collaborators can be regarded to be essentially the same as the QMD. The QMD method simulates heavy-ion reactions on an event-by-event basis and, as a consequence, incorporates many-nucleon correlations. Therefore this model offers us an opportunity to calculate not only one-body observables but also fragment formation.

Until now, however, the QMD method has not been used to study the reaction processes in low energy region and even in the Fermi energy region, $E_{lab} \sim 30$ MeV/nucleon, where E_{lab} stands for the incident energy in the laboratory frame. This, the present authors consider, is mainly due to the insufficient stability of the projectile and target nuclei constructed in the framework of the QMD method. Recently the present authors have succeeded to construct in the QMD framework the stable nuclei which maintain their stability, usually, more than 2000 fm/c.[4] Therefore now we are able to use the QMD method to study the low energy heavy-ion collision processes and also the evolution of the collision mechanism from the low energy region to the medium energy one. Since the onset of the fragmentation mechanism is considered to be an important ingredient for the collision mechanism evolution, it is very interesting and important to study how the heavy-ion collision processes are described in the framework of the QMD method in low and Fermi energy region as well as in more higher intermediate energy region.

We first reported the results of the study of the fusion reaction and its fade-out in the $^{16}O + {}^{16}O$ system in the framework of the QMD in the energy range from sub-Coulomb barrier energy up to $E_{lab} = 13.75$ MeV/nucleon. We next discussed briefly how the QMD describes the evolution of the reaction mechanism in the energy region above 13.75 MeV/nucleon up to 225 MeV/nucleon. It was shown that without two-nucleon collisions there appears the so-called fusion window like in the time-dependent Hartree-Fock approach while with the inclusion of two-nucleon collisions the low partial wave cutoff in fusion disappears. The fade-out of the fusion process with the increase of the incident energy was found to be due to the increase of the cross sections mainly of the incomplete fusion process in the whole range of the impact parameter and partly of the deep-inelastic-collision-like process in the peripheral region. The calculated fusion cross section as a function of incident energy was shown to be in good accordance with experiments.

As has been discused by many authors, the fade-out of the fusion reaction is the start of the big evolution of the reaction mechanism (RM) in 10 MeV/nucleon $\lesssim E_{lab} \lesssim$100(or 200) MeV/nucleon. We reported briefly how the RM evolves from incomplete fusion, to explosion at 225 MeV/nucleon for $b = 0fm$, to participant-spectator-like process above 150 MeV/nucleon for $b = 3fm$, and to quasi-elastic process above 75 MeV/nucleon for $b = 6fm$.

For the details of our study the reader is referred to our preprint paper, KUNS 997(Kyoto University, 1989).

REFERENCES

1. J. Aichelin and H. Stöcker, *Phys. Lett.* **176B**, 14 (1986).
2. G. Peilert, H. Stöcker, W. Greiner, A. Rosenhauer, A. Bohnet and J. Aichelin, *Phys. Rev.* **C39**, 1402 (1989).
3. G. E. Beauvais, D. H. Boal and J. C. K. Wong, *Phys. Rev.* **C35**, 545 (1987).
4. A. Ohnishi, T. Maruyama and H. Horiuchi, to be submitted to *Phys. Rev. C.*

18. Gamma Ray and Neutron Emissions from Hot Nuclei
J. Kasagi

Manuscript not received.

19. Mass Number, Energy, and Deformation Dependence of Level Density

Hiroshi Sato

Radiation Laboratory, RIKEN, Wako, Saitama 351-01, JAPAN

I. INTRODUCTION

The nuclear reaction gives us plenty informations for the studies of the reaction process and nuclear structure. The nuclear level density plays an important role in the study. However, since the conventional level density formula (derived with the saddle point method) is 'very simply nonotonic increase' function of the excitation energy, the study of the level density looks like a tedious, not-so-interesting, and time consuming work. Here reformulating the level density with the employment of the temperature dependent antisymmetrized density matrix of many fermions in a harmonic oscillator well, we show how interesting the study of the nuclear level density. And comparing the formula obtained with the conventional one, we study the applicability and limitation of the conventional level density formula.

II. NUCLEUS AS A CANONICAL ENSEMBLE

Nuclear phenomena at low excitation energy are successfully explained by shell model. On the other hand, the highly excited nuclear states (HX) formed by medium and high energy nuclear collisions have been studied mainly with thermal model. The essential difference between two models is that the shell model state is in good quantum state of the energy E and the nucleon number N, while the HX is expressed by the temperature parameter T ($= 1/\beta$) and the nucleon multiplicity N (or chemical potential μ). In this sense one may quote the microcanonical ensemble of interacting many fermions as the conventional shell model and the canonical ensemble (or grand canonical ensemble) as thermal models, though two ensembles are thermodynamically equivalent. We have studied the nuclear system both at low and high excitation energies in terms of the canonical ensemble.[1,2)]

First, we have studied the temperature dependence of the internal energy, and found that the internal energy obtained approaches to the total energy of the ground state of the HO shell model at the low temperature

limit. Second, we have calculated the temperature dependence of the exponential of the entropy, which corresponds to the number of available states of the system, and found that it approaches to the degree of degeneracy of the HO shell model ground state at the low temperature limit. The mass number dependence of the entropy for given temperatures is summarized in Fig.1. The closed shell effect on the entropy is clearly seen in Fig.1. We have also calculated the heat capacity and the root mean square radius of the system, and found that those quantities can be reasonably explainable. From these calculations we concluded that this canonical ensemble is equivalent to the HO shell model at low temperature limit.[1)]

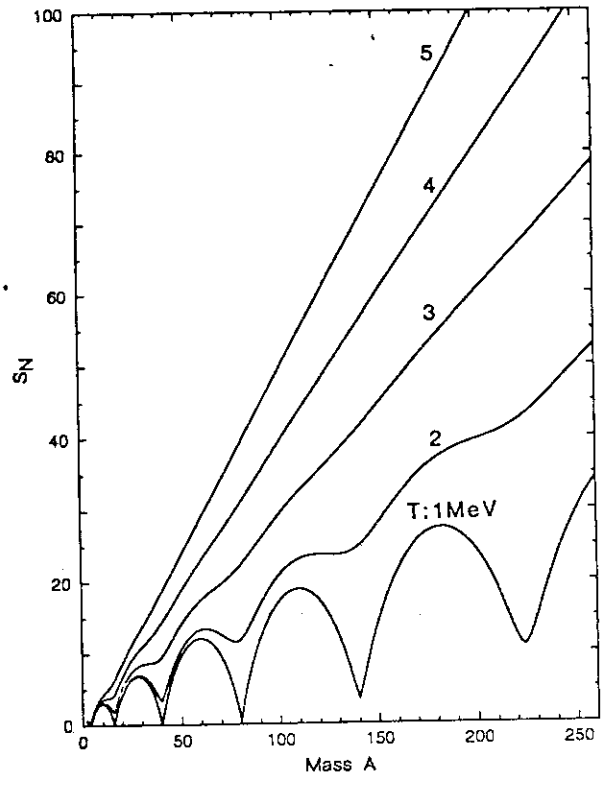

Fig.1 The mass number A dependence of the entropy S_N for given temperatures T. The mass number dependent oscillator constant $\hbar\omega = 41\,A^{-1/3}$ MeV is employed.

III. SINGLE PARTICLE SPECTRA

We also calculated the single particle emission probability from the HX with the density matrix so obtained. Then we found the single particle spectra such that

$$P_1^N(E:\beta) = \sum_{n=1}^{N} G^{\beta}(N,n) P_1^1(E:n\beta)\,,$$

$$P_1^1(E:n\beta) \underset{T\to 0}{\overset{\beta\to\infty}{\longrightarrow}} \frac{1}{N}\left[\frac{\hbar}{\pi m\omega}\right]^{3/2} \exp\left[-(E+v_0)\Big/\left[\frac{\hbar\omega}{2}\right]\right]$$

$$\underset{T\to\infty}{\overset{\beta\to 0}{\longrightarrow}} \frac{1}{N}\left[\frac{n\hbar^2\beta}{2\pi m}\right]^{3/2} \exp[-(E+v_0)n\beta]\,.$$

Here v_0 is the potential depth and ω is the harmonic oscillaotor constant as schematical shown in Fig.2. Thus we found that the particle emitted from the HX shows two typical spectra ; 1) the usual Maxwellian distribution of thermal motion at high temperature limit

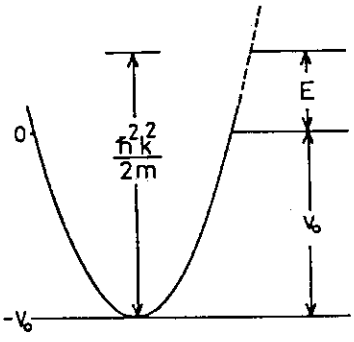

Fig.2 The schematic relationship between the particle emission energy E, the potential depth v_0, and the HO potential.

and 2) the Maxellian distribution with the effective temperature $\hbar\omega/2$ at low temperature limit. The existence of these two slope parameters is consistent with the experimental spectra observed in the medium and high energy nuclear reactions.[2)]

IV. NUCLEAR LEVEL DENSITY

Typical conventional nuclear level density formula is given by

$$\rho(N,E)=\frac{1}{\sqrt{48E}}\exp(2\sqrt{aE}) \qquad (1)$$

where E is the excitation energy. The thermodynamic temperature t is given by $t=\sqrt{E/a}$. The theoretical level density parameter a is A/15 for a free Fermi gas and A/10 for a Fermi gas in a harmonic oscillator well, while the parameter extracted from experimental data is approximated by A/8[3)]. Therefore, the applicability of the formula (1) to the real nuclear system is not clear. Furthermore, the excitation energy dependence of the parameter a is poorly known compared to its mass number dependence. Sine the exponential of the entropy (e^{S_N}) is the number of available states, the nuclear level density in the canonical ensemble is given by

$$\rho=\frac{de^{S_N}}{dE}=\beta e^{S_N}. \qquad (2)$$

Equating Eq.(1) to the values calculated with Eq.(2), we obtain the mass number dependence of the level density parameter a for given excitation energies, and summarize those in Fig.3.[1)] The parameter a is small at closed shell nuclei and large in the middle of shell nuclei. This tendency is consistent with experimental data[3)]. This excitation energy dependence is not incomptatible with recent experimental data near A = 160 obtained by Nebbia et al[4)]. However, the existence of the excitation energy dependence of the parameter a gives rise to a question on the applicability of the formula (1), because the explicit inclusion of the excitation energy dependence conflicts with the basic

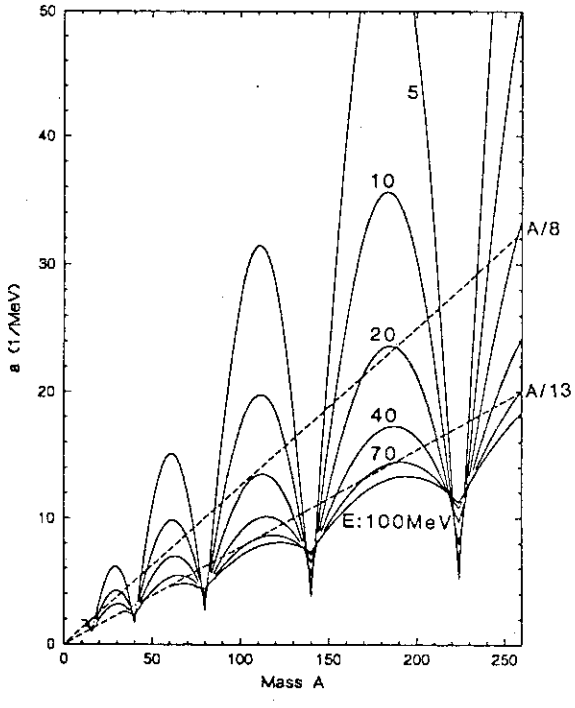

Fig.3 The mass number dependence of the level density parameter a for given excitation energies E, which is defined by equating Eq. (1) to the value calculated by using Eq. (2).

assumption of the saddle-point approximation. Therefore, we study the relationship between our treatment and the saddle-point approximation, by assuming the excitation energy E given by a simple polynomial form $E=aT^k$ of temperature, where the factor a and the order k are constants in this case. If the excitation energy E is proportional to T^2, the level density formula (2) becomes

$$\rho=\frac{a}{E}Ce^{2\sqrt{aE}} \quad \text{with } C=e^{S}N^{(T=0)}. \tag{3}$$

This formula is essentially equivalent to the conventional level density formula (1). In other words, the level density formula based on the saddle-point approximation is equivalent to the parabolic temperature dependence of the excitation energy. Therefore we examined whether the parabolic approximation for the excitation energy is adequate or not, and found that a simple polynomial (especially parabolic) form of the temperature for the excitation energy is improper to the nuclear system. This stems from the fact that nuclear single particle states are not well degenerated in comparison with the usual electron gas in the metal.

Thus we found that : 1) the level density formula based on the saddle-point approximation in the inverse Laplace transformation is not adequate in the real nuclear system, and 2) we should do with the entropy itself instead of the level density parameter a. And then we should study and discuss the mass, charge, and excitation energy dependence of the entropy from the experimental nuclear level density. In this sense, the nuclear level denity (or the entropy) plays a very important role in the interrelationship between the conventional study of nuclear states and the study of phenomena in medium and high energy heavy-ion collisions. We extend the study to the deformed HO case, and find that Strutinsky type level density distribution is obtainable with the canonical ensemble.

References:

1. H. Sato, Phys. Rev. C36, 785 (1987).
2. H. Sato, Phys. Rev. C36, 794 (1987).
3. E. Erba, U. Facchini, and E. Saetta-Menichella, Nuovo Cimento 22, 1237 (1961).
4. G. Nebbia et al., Phys. Lett. 176B, 20 (1986).

20. Recoil Mass Separator

S. Morinobu

Manuscript not received.

21. Riken On-line Isotope Separator - GARIS-IGISOL

K. Morita

Manuscript not received.

22. Experiments in Large Scale Scattering Chamber

S. M. Lee

Manuscript not received.

23. COULOMB EXCITATION OF STABLE AND UNSTABLE NUCLEI

Masumi OSHIMA*

Japan Atomic Energy Research Institute, Tokai－mura, Ibaraki 319－11

So far yrast levels have been well studied utilizing modern heavy－ion accelerators and sophisticated γ－ray detection systems. However, understanding of non－yrast excitations is still in a preliminary stage. This is due to complex decay patterns and weak feeding for each level. Basic excitations such as the two－phonon γ, β and octupole vibrational states have not in most cases been clearly identified. Such excitations, as well as the magnitude of the electromagnetic transitions connecting them to other states, are critical in distinguishing between the variety of theoretical descriptions which try to explain collective excitations in medium－mass and heavy nuclei.

Coulomb excitation selectively excites low－lying collective bands, up to spin 30 $\hbar$ in strongly deformed heavy nuclei, with cross sections that are a sensitive and direct measure of the Eλ matrix elements involved. The copious heavy－ion beams of all stable nuclei available from heavy－ion accelerators, coupled with the recent development of powerful new experimental and analysis techniques, have made it possible to measure the essentially complete set of about 200 E2 matrix elements for the lowest 30 states Coulomb excited in nuclei; that is, the magnitudes and observable signs of both the static and transition matrix elements can be measured.[1] One can derive the centroids and fluctuation widths of the electric quadrupole moments in the intrinsic frame in a model－independent manner. These intrinsic frame observables can be translated to the usual β－γ shape distribution when assuming a model. The combination of the γ－deexcitation properties plus Coulomb excitation determines the M1 transition matrix elements which probe the

single–particle degrees of freedom in nuclear structure. Thus it is possible to study the interplay and relative importance of various collective and single–particle degrees of freedom. Furthermore, it will be possible to search for multi–phonon states, such as quadrupole or octupole two–phonon states, e.g. two–γ, two–β, coupled β–γ or coupled quadrupole–octupole collective modes, which should exist but have never been clearly identified. Such studies will elucidate the coupling of these different collective modes. It may be possible to study the extent to which static octupole deformation is of importance in heavy nuclei.

One weak point in the usual Coulomb excitation is that the object nucleus is limited to a stable one. This defect can be overcome by using radioactive beams. While the application of radioactive beams has been suggested for several years, actual experiments have been few due to their low fluxes. Recent development of heavy–ion accelerators and recoil mass separators enables one to produce high–quality, heavy–ion secondary beams at fluxes and energies sufficient for Coulomb excitation studies. The inverse kinematics of primary reaction will produce high–energy recoil beams, and the recoil mass separators will separate the mass of the secondary beams with high efficiency. It should be noted that by secondary reactions we may be able to approach very exotic nuclei. The production cross section by means of primary reactions falls off very rapidly as going far off the stability line. By use of suitable combination of radioactive beam and stable target we may gain the production yields of very exotic nuclei.

One of the exciting possibilities is Coulomb re–excitation of radioactive nuclei. The secondary beam would strike a lead stopper where the beam nuclei would be Coulomb excited. It would be possible to investigate far more rich region of nuclei than possible in the present Coulomb excitation studies. It is important to measure the B(E2: $0^+ \rightarrow 2^+$) values and establish the deformations in a rich region of nuclei. In the actinide region this technique is more favorable than in other regions: fission γ–rays due to the primary reaction, which often disturb a clean spectroscopy, do not

exist at the secondary target position; the nuclei can be excited very cleanly. Studies of the Ra–Th nuclei[2,3] have revealed a new form of collective behavior at medium to high spins. In these nuclei one observes bands of states with alternating parities, linked by E1 decays. These data were interpreted as arising from reflection asymmetric nuclear states which originate from octupole shapes.[4,5] A surprising phenomenon there is that the hindrance of E1 strength, which is typically around $10^{-5}-{}^{-6}$, is restored up to around 10^{-2} single–particle units. Recently, it was shown that reflection asymmetry does generate some polarization, and causes such restoration of E1 strength.[6,7] Since the Coulomb excitation cross section is proportional to B(Eλ) in first order, largely enhanced excitation is expected for such octupole deformed states. Thus the Coulomb excitation becomes a powerful tool to investigate the octupole as well as quadrupole shape degrees of freedom in this region of nuclei.

A powerful γ–ray detection system with high efficiency, high resolution and large dynamic range is needed for such interesting physics induced by Coulomb excitation.

I would like to acknowledge Drs. Y.Gono, H.Kusakari, M.Sugawara and T.Inamura for valuable discussions on Coulomb excitation of radioactive nuclei.

References

1) D.Cline, Ann. Rev. Nucl.Part. Sci., 36, 681 (1986); and references therein.

2) W.Bonin et al., Z.Phys. **A310**, 249 (1983).

3) M.Gai et al., Phys. Rev. Lett. **51**, 646 (1983).

4) G.A.Leander et al., Nucl. Phys. **A388**, 452 (1982).

5) W.Nazarewicz et al., Nucl. Phys. **A429**, 269 (1984).

6) Y.Alhassid et al., Phys. Rev. Lett. **49**, 1482 (1982).

7) G.A.Leander et al., Nucl. Phys. **A453**, 58 (1986).